

N 70 10468

TR-DA2124

3 OCT 69

NASA CR 106529

FLIGHT DATA ANALYSIS OF POWER SUBSYSTEM DEGRADATION AT NEAR SYNCHRONOUS ALTITUDE

FIRST QUARTERLY REPORT

CONTRACT NASW-1876

PREPARED FOR:

NATIONAL AERONAUTICS AND SPACE ADMINISTRATION
OFFICE OF ADVANCED RESEARCH AND TECHNOLOGY
HEADQUARTERS, WASHINGTON, D.C.

CASE FILE
COPY

PHILCO



SPACE & RE-ENTRY SYSTEMS DIVISION
Philco-Ford Corporation
Palo Alto, California 94303

FLIGHT DATA ANALYSIS OF
POWER SUBSYSTEM DEGRADATION
AT NEAR SYNCHRONOUS ALTITUDE

FIRST QUARTERLY REPORT

Contract NASW - 1876

Prepared by:

R. J. Grant
W. T. Picciano
R. A. Reitman.

Prepared For
National Aeronautics and Space Administration
Office of Advanced Research and Technology
Headquarters
Washington, D.C.

Arvin H. Smith; Chief,
Solar and Chemical Power Systems

FOREWORD

This report concerns the electrical power subsystem performance of the Initial Defense Satellite Communication System⁽¹⁾. In particular it details the on-orbit degradation of the satellite solar arrays. The work is sponsored by the National Aeronautics and Space Administration under contract NASW-1876.

The study is being conducted in the Power and Control Engineering Department of the Philco-Ford Space and Re-entry System Division at Palo Alto, California. This department is managed by Mr. D. L. Reynard. The program is under the overall technical direction of Mr. R. J. Grant. Mr. W. T. Picciano is responsible for the mathematical techniques and approach of deriving individual cell degradation from available array telemetry parameters. Mr. R. A. Reitman has implemented the computer programming and the automatic computer plotting of the program output.

(1) Formerly Initial Defense Communication Satellite Program (IDCSP)

TABLE OF CONTENTS

<u>SECTION</u>	<u>DESCRIPTION</u>	<u>PAGE</u>
1.0	SUMMARY OF RESULTS	
1.1	Summary of Results	1-1
2.0	INTRODUCTION	
2.1	Background	2-1
2.2	Task Description and Status	2-2
3.0	SATELLITE DOCUMENTATION AND ANALYSIS	
3.1	Satellite Description	3-1
3.2	Telemetry and Instrumentation	3-15
3.3	Satellite Orbit Definition	3-27
3.4	Significance of Telemetered Parameters	3-30
3.5	The Extraction of Degradation Data	3-33
4.0	DETAILED RESULTS	
4.1	Detailed Results	4-1
Appendix A	Derivation and Accuracy of an Explicit Function for I(V)	
B	Extraction of Parameters from I-V Data	-
C	Temperature Dependence of the Parameters	
D	Degradation Analysis Computer Program	

SUMMARY OF RESULTS

SECTION 1.0

1.1 SUMMARY OF RESULTS

The primary objectives of this program are: to establish the quantitative degradation rates of the power subsystems of seventeen IDSCS spacecraft in near-synchronous orbit, to investigate the degradation of the I-V characteristics of their solar arrays, to investigate any anomalous or unexpected behavior relating to environmental damage, and to analyze all results such that the benefits of this flight experience can be applied to other current and future programs.

Based on an average assumed single cell I-V characteristic, the undegraded theoretical satellite array I-V characteristic is determined as a function of time. Telemetry data monitoring the power subsystem provides two points on the array I-V curve. The difference between the calculated and observed values of current and voltage output at these two load points produces a quantitative measure of array degradation as a function of time.

A further refinement of this difference data can be carried out with the sophisticated computer techniques developed for this program. This refinement produces a far more interesting and applicable result in terms of comparative degradation studies and future array designs. The calculated and observed array current differences are mathematically removed (i.e. made to equal zero) by varying the parameters of the assumed single cell I-V curve which makes up the array. The room temperature value of the single-cell short-circuit current is first degraded to remove the observed difference in currents for the load point on the shunted half of the array; and, with this degradation retained, the single-cell open-circuit voltage is

degraded to remove the difference at the load point of the unshunted half of the array. The validity of this technique depends on the location of these load points, which is discussed below, and the assumption of minimum I-V curve shape change, which must later be verified.

Figure 1-1 presents a summary of the cell short-circuit current degradations on the seven satellites of the first IDSCS payload. These curves normalize the detailed curve data presented in Section 4. The average degradation after 1050 days (2.87 years) is 0.897, or 10.3%. In the tentative visual fits used for this report, it is observed that the shapes of the degradation curves are remarkably consistent.

Figure 1-2 presents a normalized summary of the cell open-circuit voltage degradations over this same period. The average degradation is 0.985, or 1.5%. The curve shapes appear to be derivable from the same function, but show variation indicative of translated endpoints of that function.

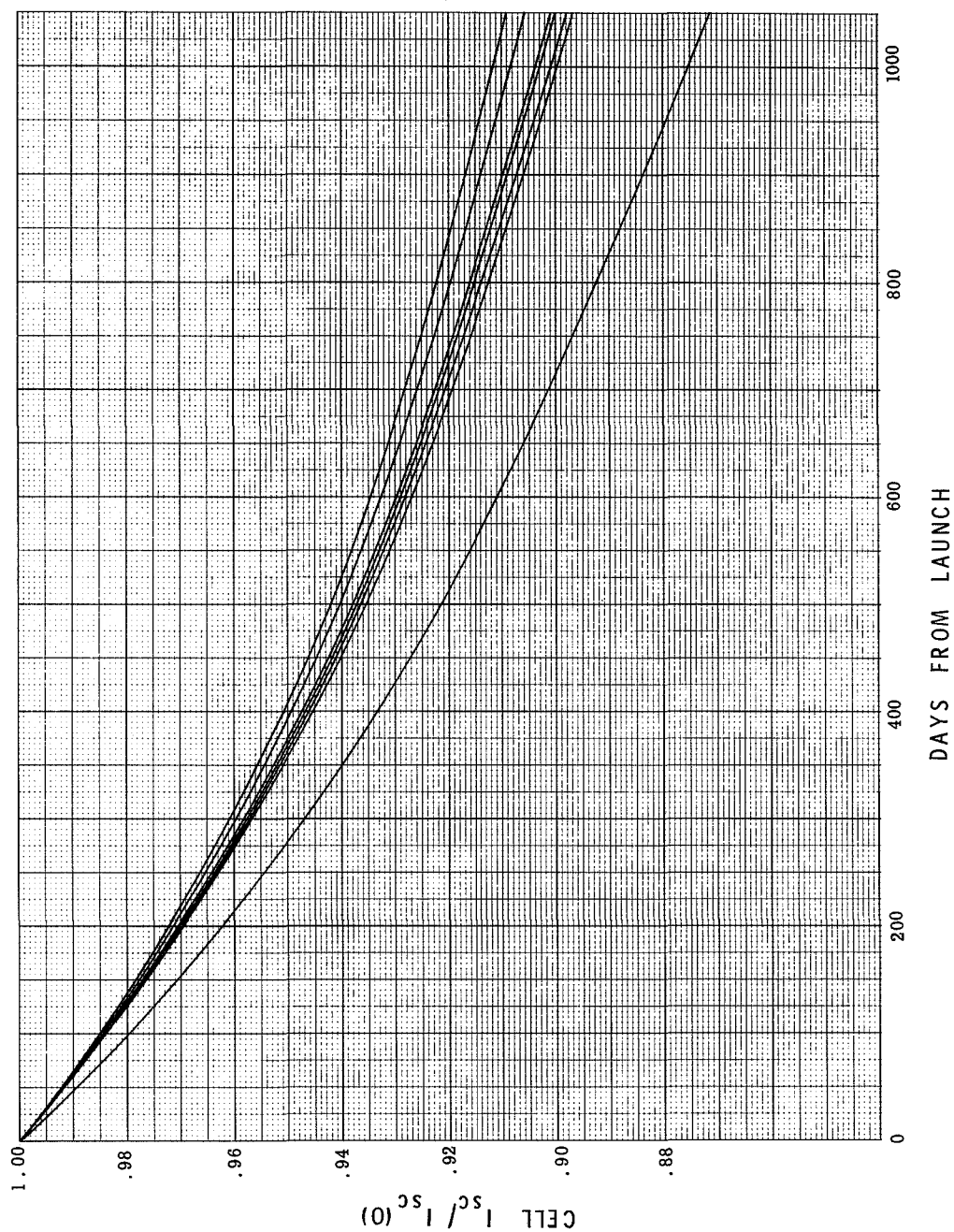


FIGURE 1-1 NORMALIZED SUMMARY OF CELL SHORT-CIRCUIT CURRENT DEGRADATION

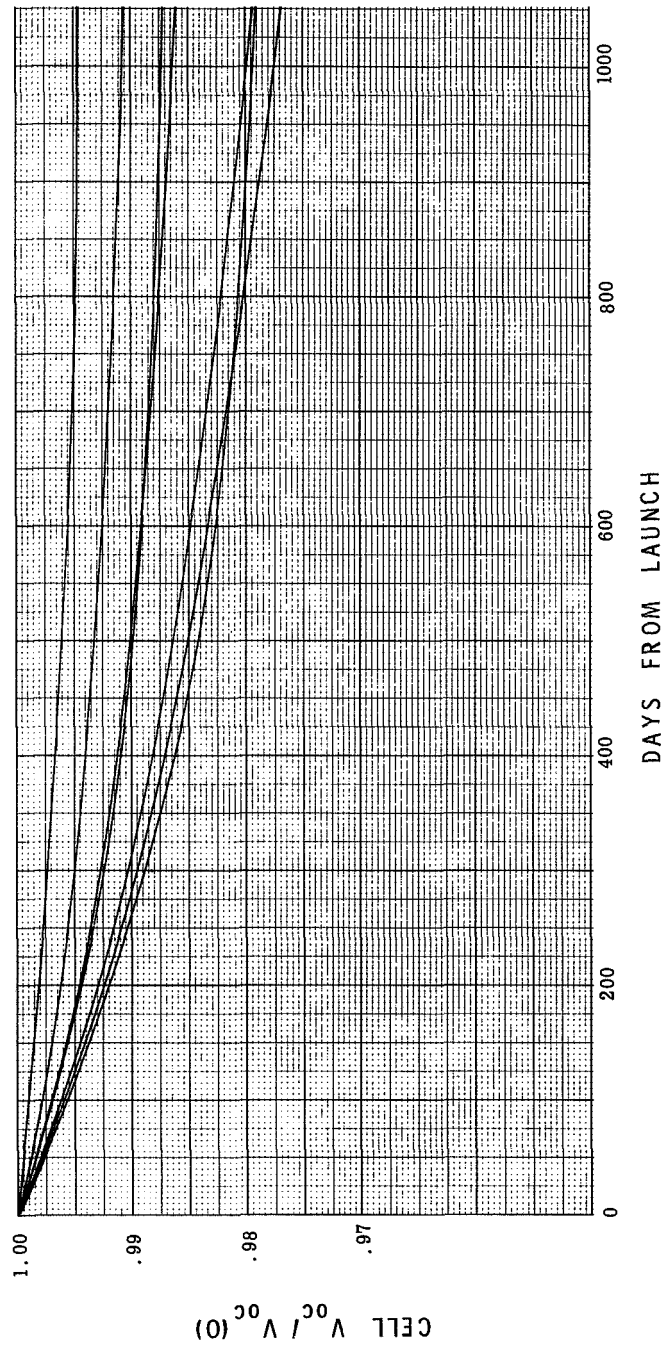


FIGURE 1-2 NORMALIZED SUMMARY OF CELL OPEN-CIRCUIT VOLTAGE DEGRADATION

INTRODUCTION

SECTION 2.0

2.1 BACKGROUND

On June 16, 1966, seven IDSCS Satellites were successfully placed in near-synchronous equatorial orbits. Subsequent to that launch eleven additional IDSCS satellites and one Despun Antenna Test Satellite (DATS) were placed in similar orbits. A comprehensive picture of solar array and solar cell degradations at synchronous altitude is now being obtained. By virtue of the large number of identical satellites, it is possible to obtain a high statistical confidence in the results. Analysis will permit a study of solar flare damage during the period 1966 - 1969. Additional analyses will compare these flight results with ground irradiation data and other flight data in an attempt to explain any anomalous behavior and allow more accurate sizing of future solar array designs.

Because of the importance of this orbit for both current and future missions, the high quality of the available telemetry data, and the nature of the results which can be obtained from this data, it is felt that the conclusions of this study will be of considerable interest to both the array design engineer and the solid-state degradation theorist. The study covers three types of activity: Design Review and Data Reduction, Data Analysis, and Advanced Data Analysis. The degree of analysis for each study phase has been established in a manner which provides balance and flexibility to the overall program. Portions of the study may be expanded or contracted depending on the results and indications of prior phases. Additionally, this study has been planned such that continuing periodic updates can be performed with a reasonably low level of effort.

The primary objectives of this program are: to establish the quantitative degradation rates of the power subsystems of seventeen IDSCS spacecraft, to investigate the degradation of the I-V characteristics of their solar arrays, to investigate any anomalous or unexpected behavior relating to environmental damage, and to analyze all results such that the benefits of this flight experience can be applied to other current and future programs.

2.2 TASK DESCRIPTIONS AND STATUS

Figure 2-1 displays a block diagram/flow chart visual summary of the program. The unification of the individual tasks towards the overall program objectives is thus clarified. Each task block contains a status indication and a reference to the location in this report of the detailed results applicable to that task.

In general, all the completed task results will appear in Sections 3.0 and 4.0. Where complex mathematics would conflict with a ready understanding of the basic analysis procedure being described, supplemental appendices are used to provide the comprehensive presentation of technical detail. Section 4.0 primarily consists of 14 figures showing the computer plots of cell I_{sc} and V_{oc} degradation points every ten days (for the first 1050 days on orbit) for each of the seven satellites of the first IDSCS payload.

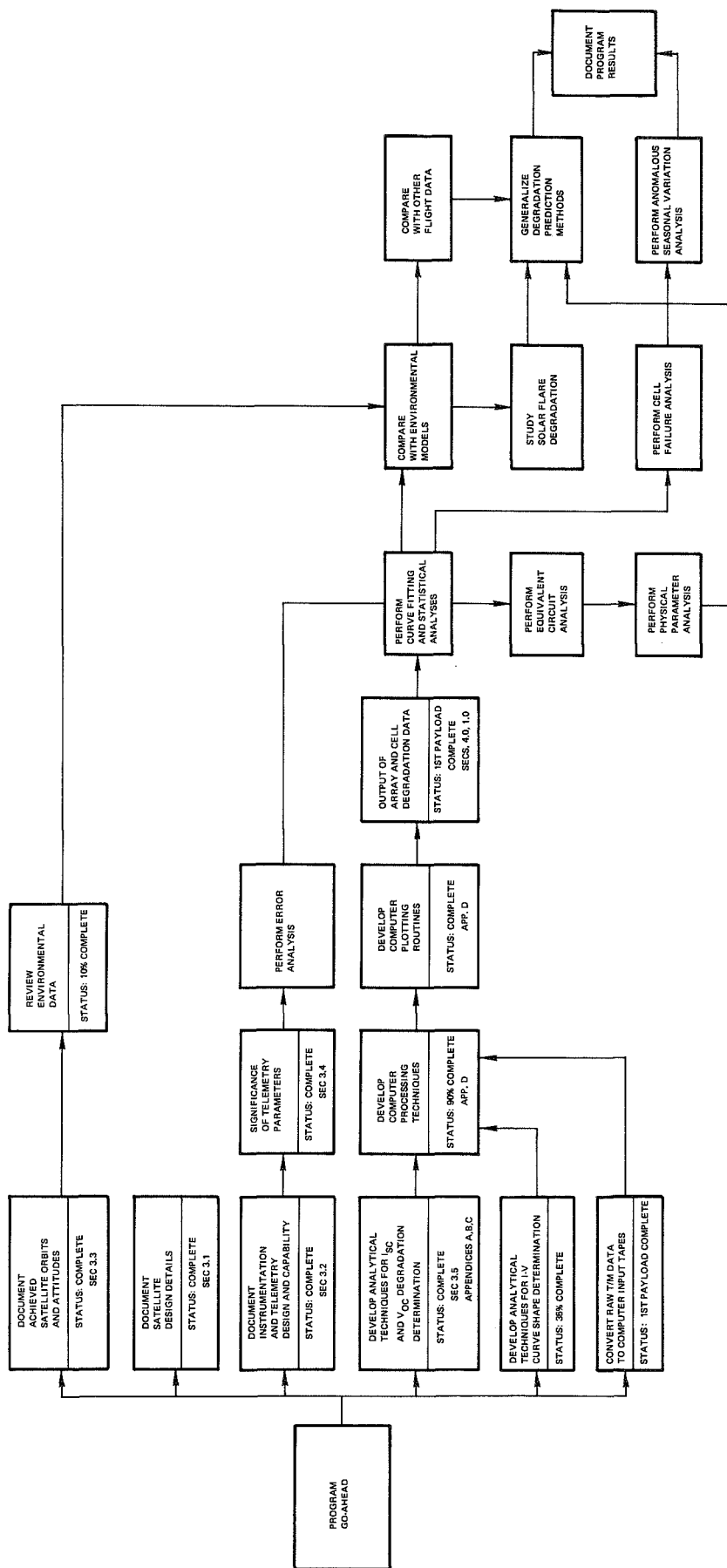


FIGURE 2-1 TASK DESCRIPTION FLOW DIAGRAM
(Includes Status and Reference Indications)

SATELLITE DOCUMENTATION AND ANALYSIS

SECTION 3.0

3.1 SATELLITE DESCRIPTION

The IDSCS satellite is an active communication repeater and is shown in Figure 3.1-1. Its shape is a symmetrical polyhedron consisting of two octahedral truncated pyramids joined by an octagonal cylindrical center section. The height of the satellite body is 31 inches, and the diameter of the circle circumscribing the octagonal cylinder is 36 inches. The satellite weighs 97 pounds and employs passive thermal control.

It is divided into four subsystems which are described in the following paragraphs. These are:

- a. Structure
- b. Power
- c. Communication
- d. Telemetry

3.1.1 Structure Subsystem

The principal components of the Structure Subsystem are the structural frame, the separation equipment, and the spin-up equipment. Solar array panels cover the external surface of the structure frame. The internal surfaces of the structure provide thermal coatings for the passive thermal control required to maintain the in-orbit operating temperatures for the communication, telemetry, and power subsystems.

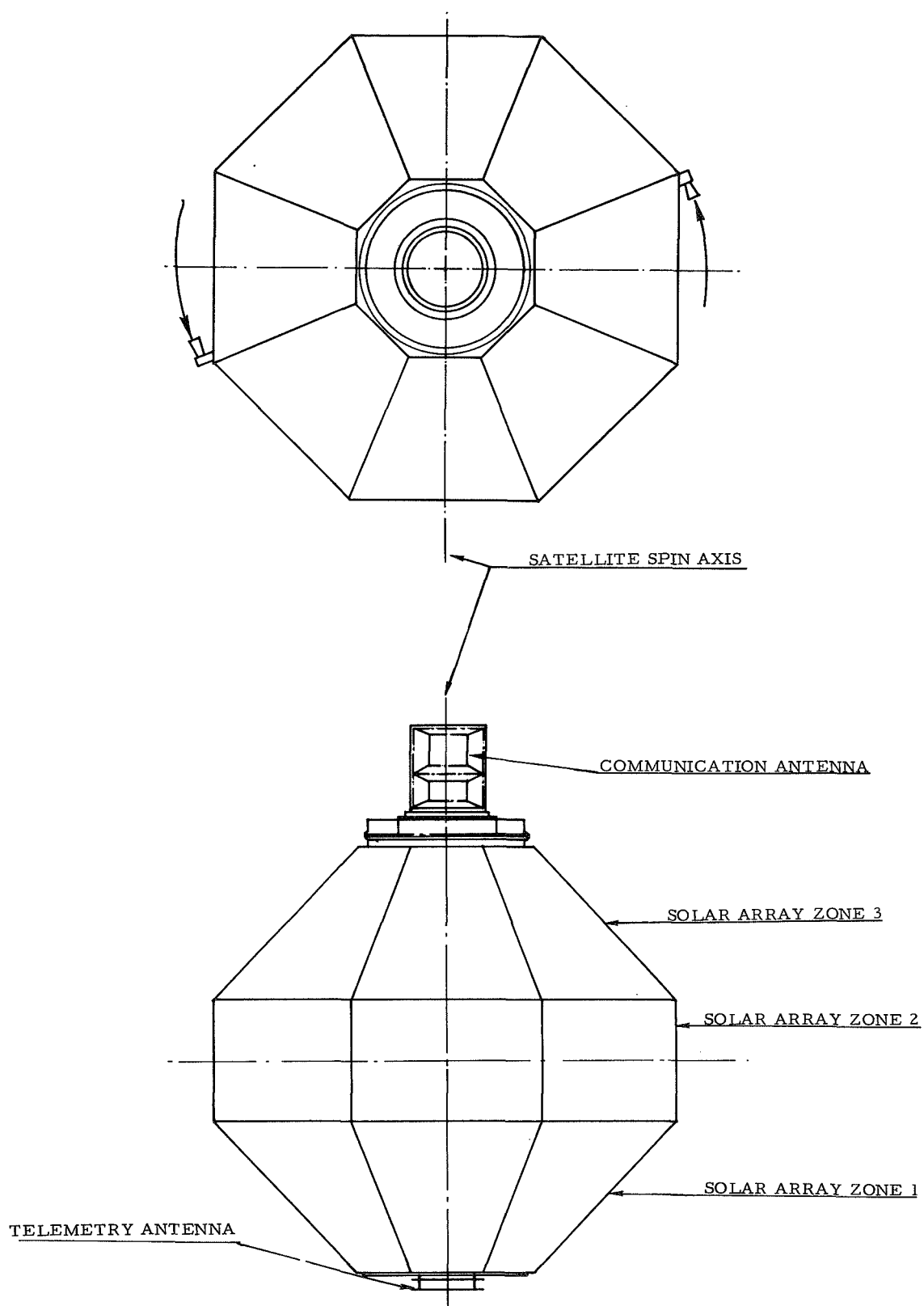


FIGURE 3.1-1 SATELLITE ENVELOPE CONFIGURATION

3.1.1.1 Structure Frame.

The structure frame provides a multifaced, symmetrical outer shell consisting of two truncated, eight-sided pyramids placed on either end of an eight-sided modified cylindrical section. The spin axis passes through the vertical apices of the truncated pyramids. The basic frame consists of a central thin-gauge magnesium alloy sheet cylinder and eight equally-spaced radial webs. An aluminum end ring is attached to each end of the cylinder to provide structural attachments and to form the octagonal shape at the truncated ends of the pyramidal sections of the body. The equipment panels are constructed of sandwich sections consisting of thin aluminum alloy facing sheets attached to an aluminum alloy hexagonal core. The four intermediate stiffening webs are fabricated from thin-gauge magnesium alloy sheets and have three large, flanged lightening holes. The central cylinder provides longitudinal stiffness to the satellite in the direction of maximum bending dictated by the horizontal position during launch.

3.1.1.2 Separation Equipment

The satellite is separated and propelled from the dispenser by the separation equipment. Attachment, with adequate circumferential clearance for the protruding communication antenna, is provided by a vee-groove clamp through a dispenser adapter ring. On a signal, two redundant ordnance bolt cutters separate the vee-groove clamp, allowing the four matched springs of the separation equipment to propel the satellite laterally from the dispenser with an acceleration of less than two g's to a velocity of three fps. As the spring faces separate from the satellite, redundant actuators actuate the satellite spin-up equipment. A clamp retention

device prevents damage to the satellite from possible rebound of the vee-groove clamp.

Both springs and satellites are unguided during separation since the expected tipoff attitude errors are less than two degrees, which the communication antenna beamwidth has been designed to accomodate.

3.1.1.3 Spin-Up Equipment

The satellite is spin stabilized at 160 revolutions per minute about its axis of symmetry by the structure subsystem cold-gas spin-up equipment which is activated immediately on separation of the satellite from the dispenser. There is no active control system.

The spin-up mechanism consists of a high-pressure nitrogen gas supply reservoir located near the satellite center of gravity, two opposed nozzles located on the outer rim of the satellite, and interconnecting lines and valves.

3.1.2 Power Control Unit

The power subsystem consists of the power control unit and the solar array, plus a radiation termination unit which automatically shuts off the power after six years in orbit. A summary of the Power Subsystem characteristics is shown in Table 3.1-1.

3.1.2.1 Power Subsystem

A simplified block diagram of the Power Control Unit (PCU) is shown in

TABLE 3.1-1

SUMMARY OF POWER SUBSYSTEM CHARACTERISTICS

1. Bus Regulation:	29.4 ± 0.2 VDC
2. Bus Ripple:	300 MV P-P; 0-50 KHz
3. Bus Impedance:	Less than 1Ω ; 0-50 KHz
4. Total Load:	28.75 Watts Maximum
5. Load Control:	Automatic Turn-On and Turn-Off Based on Available Power
6. Life:	Support Communications for 3 years Minimum Support Communications and Tele- metry for 1.5 Years Minimum

Figure 3.1-2. The function of the PCU is to regulate and distribute the solar array power and to provide telemetry inputs on the performance of the electrical power subsystem. The PCU performs the following specific functions:

- a. Regulates the main power bus voltage
- b. Provides automatic disconnect and reconnect of the telemetry subsystem as dictated by the solar array power delivery capability.
- c. Provides automatic disconnect and reconnect of the communication subsystem as dictated by the solar array power delivering capability.
- d. Provides telemetry monitoring of current, voltage, and temperature to allow operational analysis of the subsystem.

Regulation is accomplished by means of a partial shunt regulator which senses bus voltage and maintains the bus at 29.4 ± 0.2 volts. The shunt is tapped near the electrical center of the solar array and requires a minimum of power to be dissipated in the regulator.

When there is insufficient power to operate both the communication and telemetry subsystems, a bus undervoltage condition occurs. This undervoltage is redundantly sensed and the telemetry load is removed by solid-state switching. Should the undervoltage condition continue to exist, as would occur during eclipse, the communications load is removed. A resistive load equal to the communications load is then substituted across the main power bus. The voltage across this dummy load is monitored, and when sufficient power becomes available to assure that the solar array can support the communication subsystem, the substitute load is removed and communications is energized. If, after energizing

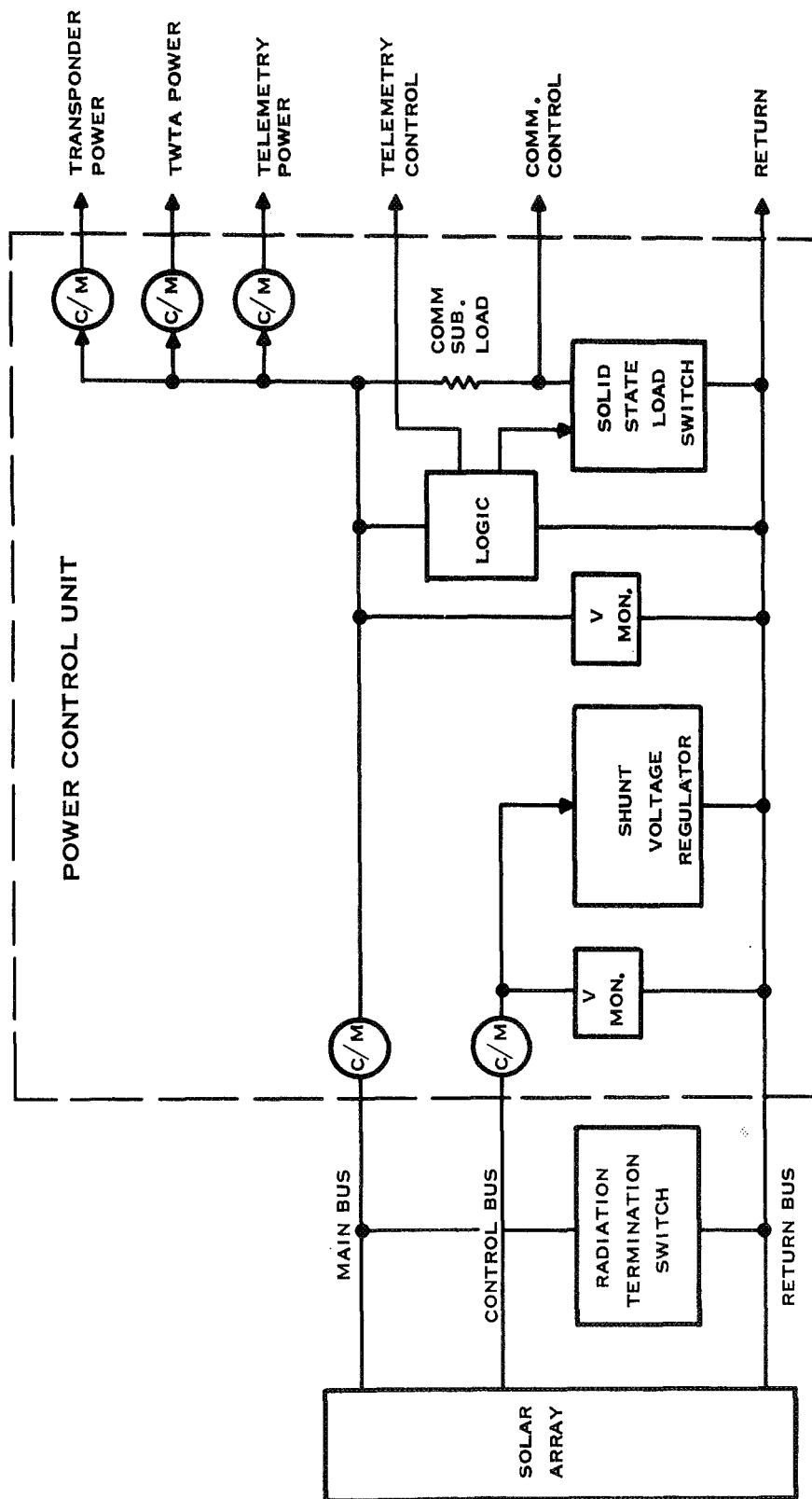


FIGURE 3.1-2 POWER SUBSYSTEM BLOCK DIAGRAM - SIMPLIFIED

communications, sufficient power becomes available to support telemetry, that subsystem also is reactivated.

3.1.2.2 Solar Array

The solar array is designed to provide electrical power to the spacecraft during illuminated periods. The start-of-life power developed by the array is nominally 45 watts.

The system power requirements are as follows:

	<u>Watts</u>
Communication Subsystem	22.0
Telemetry Subsystem	4.5
Power Control Unit	<u>3.25</u>
Total System Consumption	29.75

The solar array is made up of 16 trapezoidal and eight rectangular panels. The trapezoidal panels have an electrical arrangement of 4 cells in parallel by 84 cells in series; the rectangular panels, 4 cells in parallel by 76 cells in series. The 24 panels are connected in parallel and electrically isolated by redundant diodes. The array is approximately center tapped to permit regulation.

The cells are 1 x 2 cm N on P gridded silicon cells with solder-dipped silver-titanium grids and electrodes. The N contact is the bar type and is located along the 1 cm edge of the cell. The cells are nominally 0.356 mm (14 mils) thick.

For purposes of thermal control and radiation protection, each cell is fitted with a coverslide. The coverslides are 0.508 mm thick (20 mils) and are made from Corning 7940 fused silica. They employ an anti-reflective coating and a blue-reflecting interference filter with a cut-on wavelength of 435 millimicrons. The coverslide is primed with Dow XR-6-3466 and bonded to the cell with Dow XR-6-3489 catalyzed 1:10.

The cells are interconnected using 0.051 mm (2 mils) dead soft copper. These interconnects are plated with 8 microns (0.3 mils) of 60/40 tin-lead to facilitate soldering into modules. The modules are ultimately bonded to a fiberglass insulator with Dow RTV-511 adhesive.

3.1.3 Communications Subsystem

3.1.3.1 Transponder

The transponder is a heterodyne repeater receiving in the 8 GHz band and transmitting in the 7 GHz band. The transponder consists of a single wide-band receiver with a 10 db noise figure and a hard limiter, two transmitters with two 3.0 watt traveling-wave-tube amplifiers, two frequency generators which generate crystal-controlled local oscillator and beacon signals, a DC-DC power converter, and a redundancy control. Figure 3.1-3 shows the block diagram of the transponder.

The transponder receives incoming signals, consisting of a composite signal of up to four independent angle-modulated communications signals. The transponder translates the incoming signals to the transmit band and amplifies them. An internally generated beacon signal, coherently related to the local oscillator signals used in the translation process, is

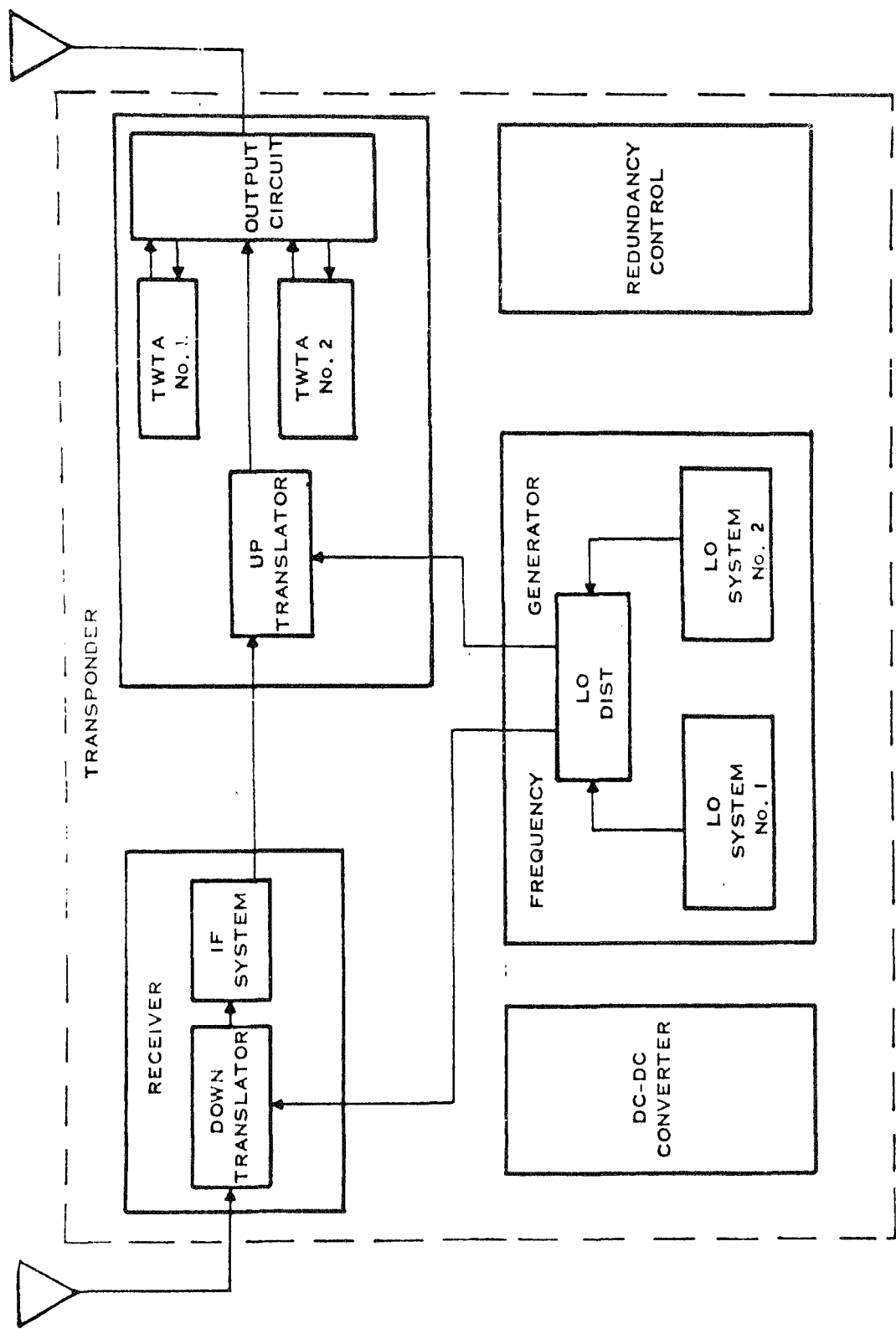


FIGURE 3.1-3 TRANSPONDER SUBSYSTEM BLOCK DIAGRAM, SIMPLIFIED

combined with the communication signals. This composite signal of communications carriers and one beacon carrier is then fed to the antenna for retransmission.

The transponder continuously transmits a 100-milliwatt beacon carrier at a frequency adjacent to the communications band. This signal is used by the ground station for acquisition and pointing the antenna at the satellite. The beacon carrier is capable of being modulated with a satellite identification signal and/or a narrow-band telemetry signal.

Coherent local oscillator signals (for the down-translator and up-translator) are generated in one of two sequentially-redundant local oscillators within the frequency generator unit and distributed as required by the local oscillator distribution subassembly. Control of the sequential local oscillator switching is accomplished by the redundancy control unit.

Regulated power is supplied to other transponder subassemblies by the DC/DC converter unit, which draws its power from the satellite power subsystem. Redundant TWTA's contain internal DC/DC converters.

The redundancy control monitors key electrical parameters, such as transmitter output power, and decides when to switch in the second frequency generator and/or TWTA.

3.1.3.2 Telemetry Subsystem

A simplified block diagram of the telemetry subsystem is shown in Figure 3.1-4. Elements of the subsystem include a telemetry generator, transmitter, power converter, antenna, sun-angle sensor, and temperature sensors.

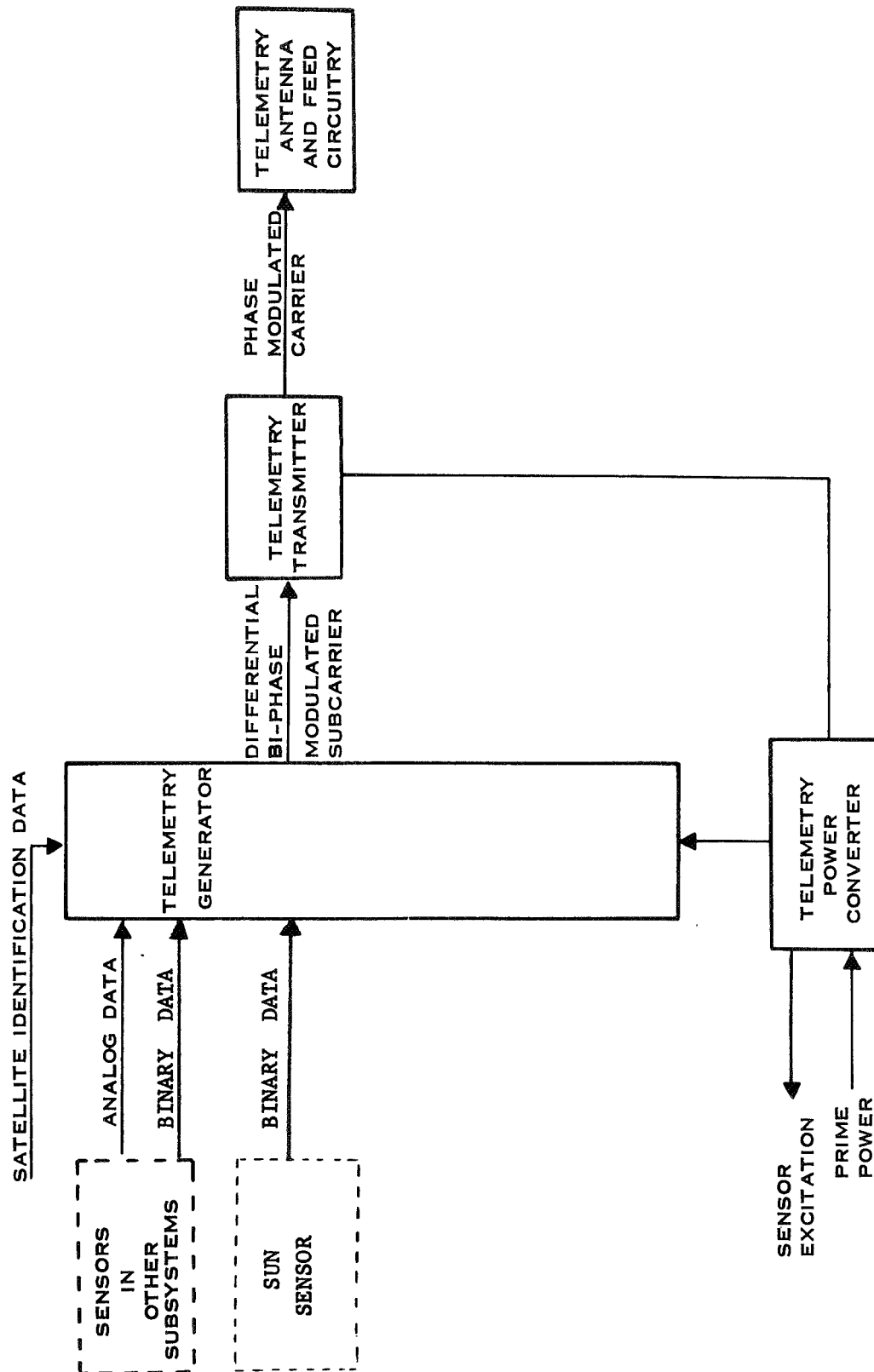


FIGURE 3.1-4 TELEMETRY SUBSYSTEM BLOCK DIAGRAM - SIMPLIFIED

The subsystem furnishes satellite identification, processes 56 analog telemetry signals and 18 binary signals, and transmits the data over a PCM/PSK/PM link to a 60-foot antenna at Ft. Dix, Camp Roberts, and to Air Force tracking stations. The satellite telemetry subsystem is compatible with existing ground station decommutation equipment. Detailed performance characteristics of the subsystem are listed in Table 3.1-2.

A binary-coded input identifies up to 64 satellites. Satellite telemetry instrumentation is used to verify operational status and performance of satellite subsystems and for diagnostic analysis during malfunction conditions. Significant satellite and equipment temperatures, voltage/current/power levels, and operational status are instrumented with appropriate signal conditioning. The signals are multiplexed in the telemetry generator, analog signal levels are converted to digital signals, and the serial data stream is programmed for pulse code modulation (PCM). The PCM data are differentially biphased and modulate a crystal-controlled, phase-modulated 400-Mc transmitter. The transmitter feeds a flat plate antenna with a pattern similar to the communication antenna, but with broader coverage.

The ground data channel signal-to-noise ratio is 11 db at the bit rate of 256 bps. Using a 60-foot receiving antenna, this is well above the 6-db value considered as a minimum safe link margin.

TABLE 3.1-2

SUMMARY OF TELEMETRY
SUBSYSTEM CHARACTERISTICS

1. Data System: Binary (NRZ) PCM
2. Number of input variables: 74 maximum
 - 18 Binary
 - 56 Analog
3. Frame synchronization: Zero plus 7-bit Barker (01110010)
4. Frame length: 64 words
5. Word length: 8 bits
6. Data quantization: 6 bits
7. Data sample rate: Once every two seconds
8. Word synchronization: 2 bits (11)
9. Frame format:
 - Frame synchronization
 - Satellite identification code
 - 18 1-bit variables
 - 56 6-bit variables
 - 3 6-bit calibration references
10. Subcarrier frequency: 1024 cps \pm 0.05%
11. Subcarrier modulation: Differential biphase
12. Bit rate: 256 bps
13. Carrier frequency: Crystal-selectable, 400 to 401.5 Mc
14. Carrier stability: $\pm 5 \times 10^{-6}$
15. Carrier modulation: Phase, ± 1.0 radian peak
16. Transmitter output power: 250 mw minimum
17. Antenna gain: 0 to -6 db, depending on aspect
18. Antenna polarization: Right-hand circular

3.2 TELEMETRY AND INSTRUMENTATION DETAILED DESCRIPTION

3.2.1 Purpose

The basic requirements of the telemetry subsystem include data measurements, satellite identification, engineering evaluation readouts, and transmission of these signals to ground station terminals by an independent RF link.

The data measurements include sun angle and satellite temperature data. Sun angle data is used for satellite attitude determination to measure the effects of orbit injection, separation and spin stabilization errors and long-term magnetic moment effects on satellite spin axis precession. Temperatures are measured throughout the satellite, subsystems, and equipments.

Satellite identification is furnished to provide unambiguous readout of up to 64 satellites.

The engineering evaluation telemetry instrumentation monitors equipment and subsystem performance throughout the satellite. This data serves the following purposes:

- a. Operational Status Verification - Typically, the switching modes of redundancy control unit.
- b. Performance Verification - Functional parameters, together with temperature data, are instrumented to verify proper operation, adequacy of design margins, and the development/production test program in simulating the orbital environment.

- c. Degradation - The gradual shift of critical functional parameters, such as solar array output power, gives advance warning of degraded performance or increased probability of malfunction, for planning of subsequent launch schedules.
- d. Diagnostic Analysis - In the event of operational malfunction or failure, telemetry instrumentation serves to isolate the problem area, reports parameter changes in that circuit or related equipments, and furnishes information for ground test simulation of the problem. Analysis of this data leads to modifications improving the performance or reliability of subsequent equipments.

3.2.2 Design Philosophy

The detail design characteristics of the subsystem were selected to provide adequate telemetry data yield at minimum cost, within present technology and using existing ground station equipment wherever practical. To satisfy these goals, the frame format and synchronization techniques were chosen to conform with the Advent program using presently available ground facilities. Accordingly, the output of the telemetry generator is a serial PCM pulse train, differential bi-phase modulating a 1024 cps subcarrier at a rate of 256 bits per second. The word length is 8 bits. The first two bits are word synchronization, and the last six bits are a binary coded representation of the information, most significant bit first. The frame synchronization code (01110010) conforms to that accepted by the Advent ground decommutation equipment.

In the interest of minimizing complexity, the telemetry subsystem provides a 64-word output frame without subcommutation features. The frame total

of 64 words was chosen as ample capacity for the satellite. The telemetry instrumentation points were selected to measure critical subsystem performance requirements.

3.2.3 Detailed Description

3.2.3.1 Telemetry Generator

The generator uses integrated circuits to provide a reliable, efficient equipment with small volume and light weight. The unit was designed for 8-bit accuracy which, while not required for this application, offers inherent flexibility for future program requirements.

Design parameters are compatible with existing ground station facilities as previously described. The generator accepts up to 56 analog data inputs and 18 binary data inputs. Satellite identification inputs are inserted by a pre-wired external connector. The data input signals are time-multiplexed, analog signals are digitized, and the signals are synchronized by an internal clock oscillator. The data signals, satellite ID inputs, and internal calibration channels are programmed into a serial NRZ-PCM binary bit stream. The calibration channels are used for reference purposes in subsequent ground data reduction. The PCM data bi-phase modulates a 1024 cps subcarrier, to form the transmitter modulation signal.

3.2.3.2 Telemetry Transmitter

The transmitter utilizes a crystal-referenced temperature-compensated oscillator driving a buffer amplifier. The signal is frequency-multiplied,

phase modulated, with frequency doublers and power amplification as required to achieve the required 400 MHz output. Due to the requirement for selected frequencies within the operating band, provisions are made for factory tuning of the transmitter using different crystals to achieve the desired RF channel.

3.2.3.3 Power Converter

The DC/DC power converter is used to isolate the telemetry subsystem from electrical transients, noise in the primary power source; to eliminate ground loops; and to provide the specific voltage levels and regulation required for optimum performance and efficiency of the subsystem elements.

The converter is designed to operate over a +24 to +40 VDC primary source voltage range, in excess of the normal +24 to +30 VDC range, to permit the telemetry subsystem to monitor power source regulator malfunctions. The converter is designed for current-limiting in the event of a telemetry subsystem malfunction, so the primary communications function of the satellite will not be jeopardized. The converter uses pulse-width modulation to achieve regulation at optimum efficiency. The converter provides power for the transmitter, generator, attitude sensor, and all temperature sensors used in the satellite. Primary power to the subsystem elements is routed to the telemetry generator and distributed through the generator system interface connectors. Since temperature sensor accuracy is a direct function of reference voltage regulation, additional regulation is used for the +6 VDC supply.

3.2.3.4 Instrumentation

A complete listing of satellite instrumentation is shown in Table 3.2-1. A detailed description is provided only for the sensors pertinent to this study.

3.2.3.4.1 Voltage Monitors

The voltage monitors are simple resistor dividers providing 0-3 volt analog output over their specified monitor range. The main bus voltage monitor is shown in Figure 3.2-1, the control bus voltage monitor in Figure 3.2-2. The following accuracy and stability requirements are specified:

Initial Accuracy (all conditions) $\pm 2\%$

Stability (3 years) $\pm 2\%$

3.2.3.4.2 Current Monitor

The current monitors are of the magnetic amplifier type. They derive their excitation from a common square wave inverter operating at 3 kHz. This constant volt-second excitation is impressed across the primary of the current monitor transformer. The DC current being monitored flows in the secondary of the transformer modulating the drive in the primary. The modulated drive is rectified by a full wave bridge and filtered by an output capacitor. Calibration of the current monitor is accomplished by a select-at-test load resistor. A unique feature of the design is a negative feedback winding which tends to linearize the output. A schematic of the inverter and monitors is shown in Figure 3.2-3.

TABLE 3.2-1

TELEMETRY INSTRUMENTATION SCHEDULE

Channel Nomenclature	Function	Normal Parameter Value	Maximum Parameter Variation	Sensor Signal Conditioner
Main bus voltage	Monitor solar array perf.	24 to 30v	24 to 50v	Resistive divider
Control bus voltage	Monitor voltage limiter perf.	0 to 15v	Full scale: 0 to 25v	Resistive divider
Main bus current	Monitor solar array perf.	1A to 1.2A	0 to 2A	Magamp
Control bus current	Monitor volt. limiter perf.	0 to 1A	0 to 1A	Magamp
TWTA primary current	Monitor TWTA performance	0.5 to 0.65A	0 to 0.8	Magamp
Transponder primary curr.	Monitor trans. performance	0.22 to 0.27A	0 to 0.5A	Magamp
Telemetry S/S primary curr.	Telemetry performance	0.15 to 0.21	0.1 to 0.3A	Magamp
Comm. on-off control status	Monitor comm. control status	0 to 1vdc off 5 to 15vdc on	N/A	Resistive divider
Power control unit temp.	Monitor operational temp.	0 to +90°C	-26 to +100°C	Temp. sensor
Solar panel zone #1 temp(hi range)	Monitor operational temp.	-18 to +50°C	-18 to +60°C	Temp. sensor
Solar panel zone #2 temp(hi range)	Monitor operational temp.	-18 to +50°C	-18 to +60°C	Temp. sensor
Solar panel zone #3 temp(hi range)	Monitor operational temp.	-18 to +50°C	-18 to +60°C	Temp. sensor
Solar panel zone #1 temp(lo range)	Monitor operational temp.	-68 to -18°C	-79 to -18°C	Temp sensor
Solar panel zone #2 temp(lo range)	Monitor operational temp.	-68 to -18°C	-79 to -18°C	Temp. sensor
Solar panel zone #3 temp(lo range)	Monitor operational temp.	-68 to -18°C	-79 to -18°C	Temp. sensor
Sun Angle Sensor	Measure sun angle to satellite spin axis	+25°	+25°	Photo diode

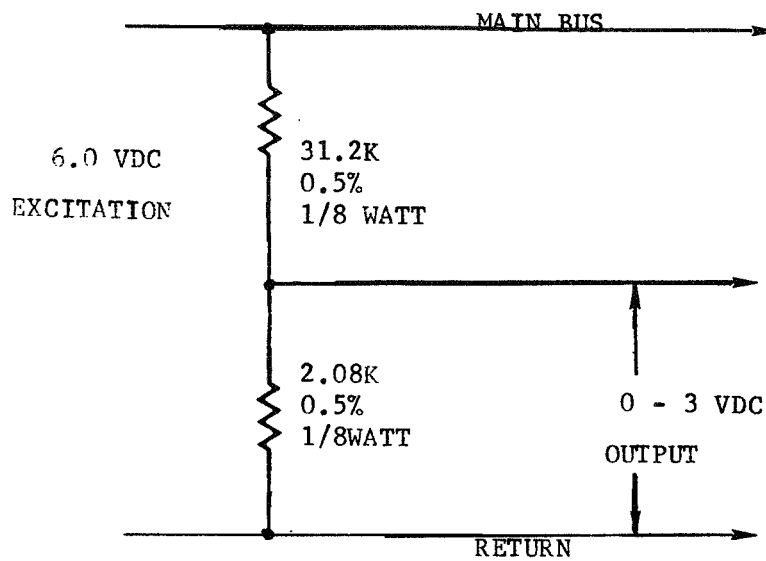


FIGURE 3.2-1 MAIN BUS VOLTAGE MONITOR

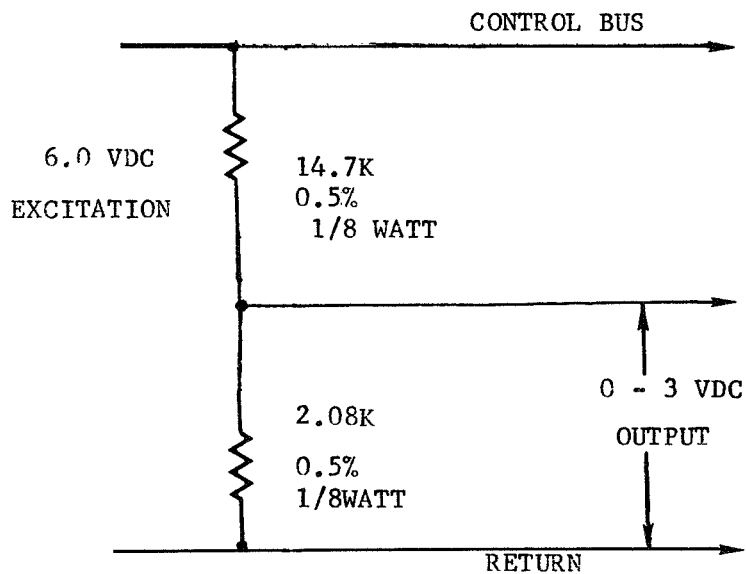


FIGURE 3.2-2 CONTROL BUS VOLTAGE MONITOR

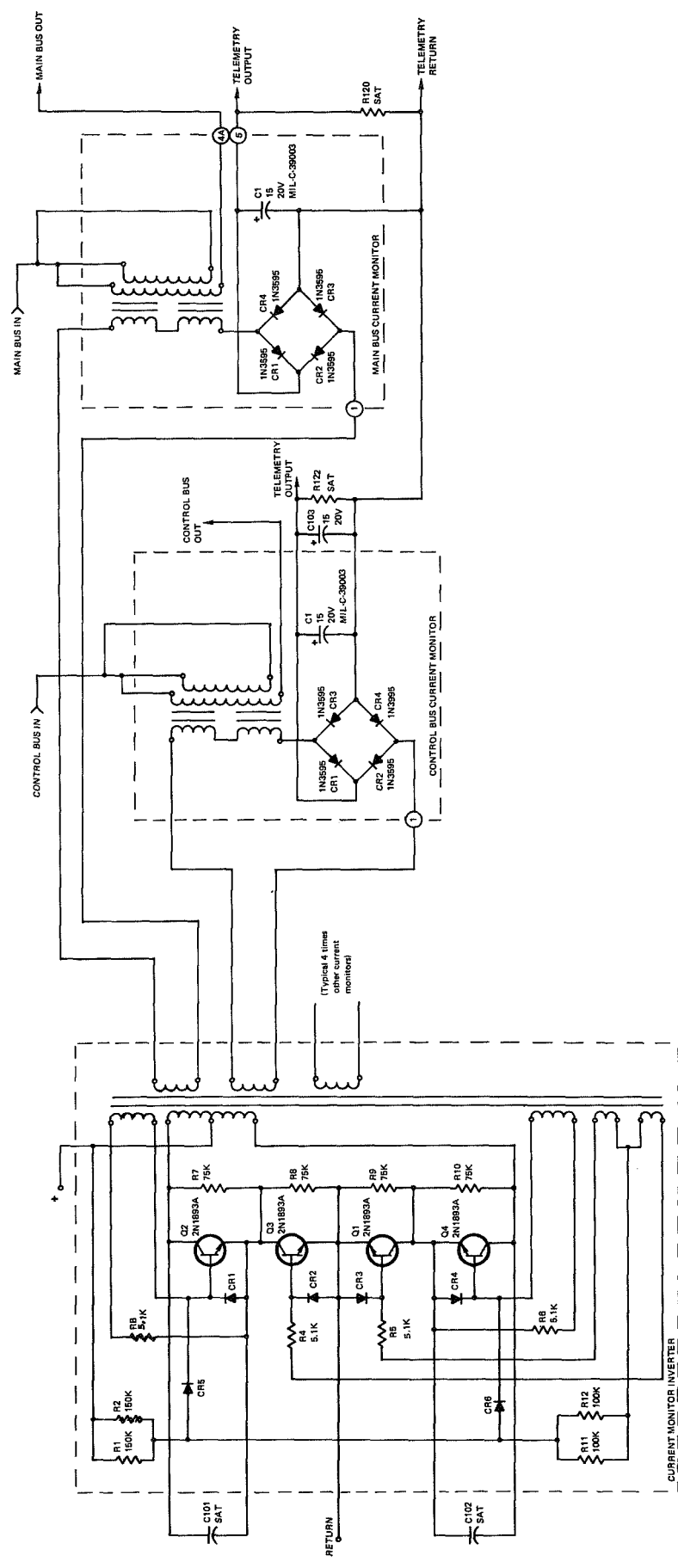


FIGURE 3.2-3 CURRENT MONITORS AND INVERTER SCHEMATIC

The following accuracy and stability requirements are specified:

Initial Accuracy (all conditions)	$\pm 2\%$
Stability (3 years)	$\pm 2\%$

3.2.3.4.3 Temperature Monitors

Temperature monitoring is accomplished by the thermistor-resistor networks shown in Figures 3.2-4 and 3.2-5. Each of the three solar panel zones contains one of each monitor. Two are required to adequately cover the entire solar panel temperature range.

The following accuracy and stability requirements are specified:

Initial Accuracy (all conditions)	$\pm 3^{\circ}\text{C}$
Stability (3 years)	$\pm 3^{\circ}\text{C}$

3.2.3.4.4 Sun Angle Sensor

The following section describes the Sun Angle Sensor used in the IDCSP program. This Sun Angle Sensor measures the angle of incident sunlight with respect to the satellite spin axis and converts this angle to a digital word. It consists of two light detector heads, one mounted near each pole of the satellite, and the associated Sun Angle Sensor Electronics.

On a spin-stabilized spacecraft, the spinning action is utilized to perform a detector scanning function. The field of view of the detector head is a fan-shaped wedge, $96^{\circ} \times 3^{\circ}$. Incident solar illumination passing through

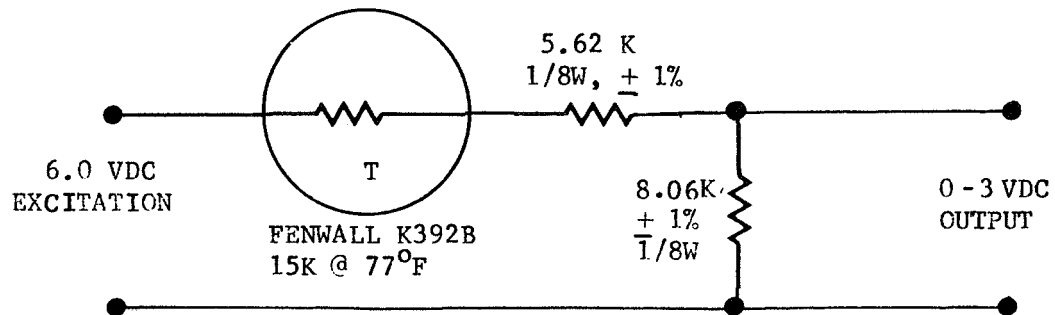


FIGURE 3.2-4 TEMPERATURE SENSOR (HIGH RANGE)

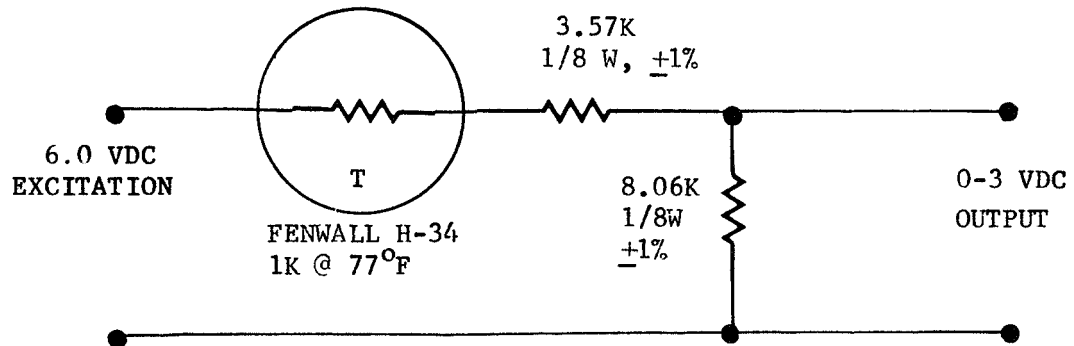


FIGURE 3.2-5 TEMPERATURE SENSORS (LOW RANGE)

an optical slit and 8-bit Gray-Code mask impinges on a photosensitive semiconductor diode. When light shines on the masked diode junction, a decrease in the diode resistance changes a bias current. The resulting signal is amplified as a digitized signal which measures the angle between the sun and the plane of the sensor.

The detector signals activate the associated Sun Angle Sensor Electronics circuitry. The output signal to the Telemetry Generator is an 8-bit digital word, 7 bits representing the angle of the sun in respect to the satellite spin axis and the 8th bit indicating which of the two detectors is being energized. A "0" in the 8th bit indicates detector #1 is being energized and a "1" indicates detector #2 is operating. To eliminate the ambiguous reading when incident illumination is near 90 degrees, detector #1 is physically mounted in a plane 90 degrees away from detector #2.

The block diagram of the Sun Angle Sensor as shown in Figure 3.2-6.

The following accuracy and stability requirements are specified:

Accuracy $\pm 0.46^{\circ}$

Stability $< 0.1^{\circ}$

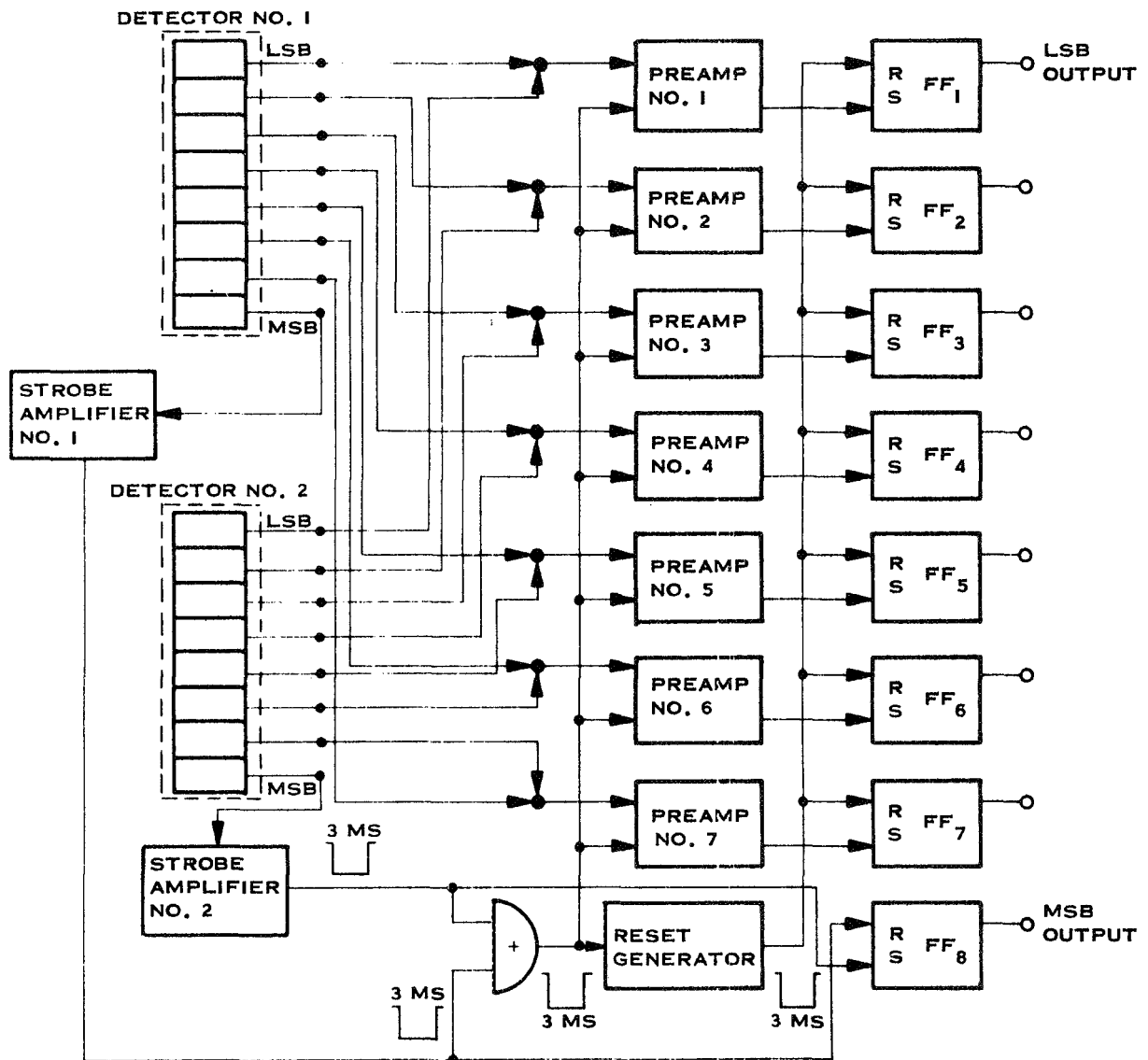


FIGURE 3.2-6 SUN ANGLE SENSOR BLOCK DIAGRAM

3.3 SATELLITE ORBIT DEFINITION

Three launches are considered in this study: The first (7 satellites) on 16 June 1966; the third (8 satellites) on 18 January 1967; and the multiple payload* (4 satellites) on 1 July 1967. The second launch self-aborted shortly after liftoff due to structural failure of the booster fairing. The first and third launches achieved slightly subsynchronous circular equatorial orbits. The multiple payload orbit was similar, but inclined seven degrees due to the desire to increase the total payload weight.

The nominal orbits for the three launches are given in Table 3.3-1. The individual satellite orbits differ slightly because each has a slightly different initial velocity to insure separation and eventual distribution around the earth.

Table 3.3-2 shows the achieved spin axis angles to the ecliptic plane for the first and third launches. Included also are the projected three-year angles. This detailed data is not available for the multiple payload, but simplified reduction of sun angle sensor data shows that spin axis angles for Satellites 9331, 9332, and 9333 are normal to the orbit plane within one degree. No sun angle data is available on 9334, the Despun Antenna Test Satellite (DATS). There is no reason to believe, however, that its attitude error exceeds one degree. A definition of angles is given in Figure 3.3-1.

*This launch included Dodge and LES-5.

TABLE 3.3-1
SATELLITE ORBITS

Orbital Parameter	1st Launch 16 June 1966	3rd Launch 18 Jan 1967	MPL 1 July 1967
Apogee - nautical miles	18,606	18,330	18,228
Perigee - nautical miles	18,205	18,161	18,191
Eccentricity	0.0092	0.0039	0.00086
Inclination - degrees	0.042	0.41	6.998
Period - Minutes	1,350	1,335	1,332

TABLE 3.3-2
SATELLITE ATTITUDES

Satellite Identification	X Component Degrees	X Component Degrees	3 Year X Component Degrees	3 Year X Component Degrees
1st Launch				
9311	-1.08	-0.04	-1.50	+0.05
9312	-0.12	+0.93	-1.00	+0.78
9313	+0.22	-0.13	+1.70	0.00
9314	-0.44	-1.10	-0.44	-1.10
9315	+0.61	+0.11	+0.70	-0.40
9316	+0.79	-0.03	-0.30	+0.05
9317	+1.11	+1.02	-0.40	+0.86
3rd Launch				
9321	-1.12	-0.37	-1.12	-0.37
9322	+1.99	-0.35	+1.99	-0.35
9332	+1.10	+1.26	+1.10	+1.26
9324	+1.36	-0.57	+1.36	-0.57
9325	-0.50	+0.27	-0.50	+0.27
9326	+1.42	0.00	+1.42	0.00
9327	-1.06	+0.30	-1.06	+0.30
9328	+0.37	-1.57	+0.37	-1.57

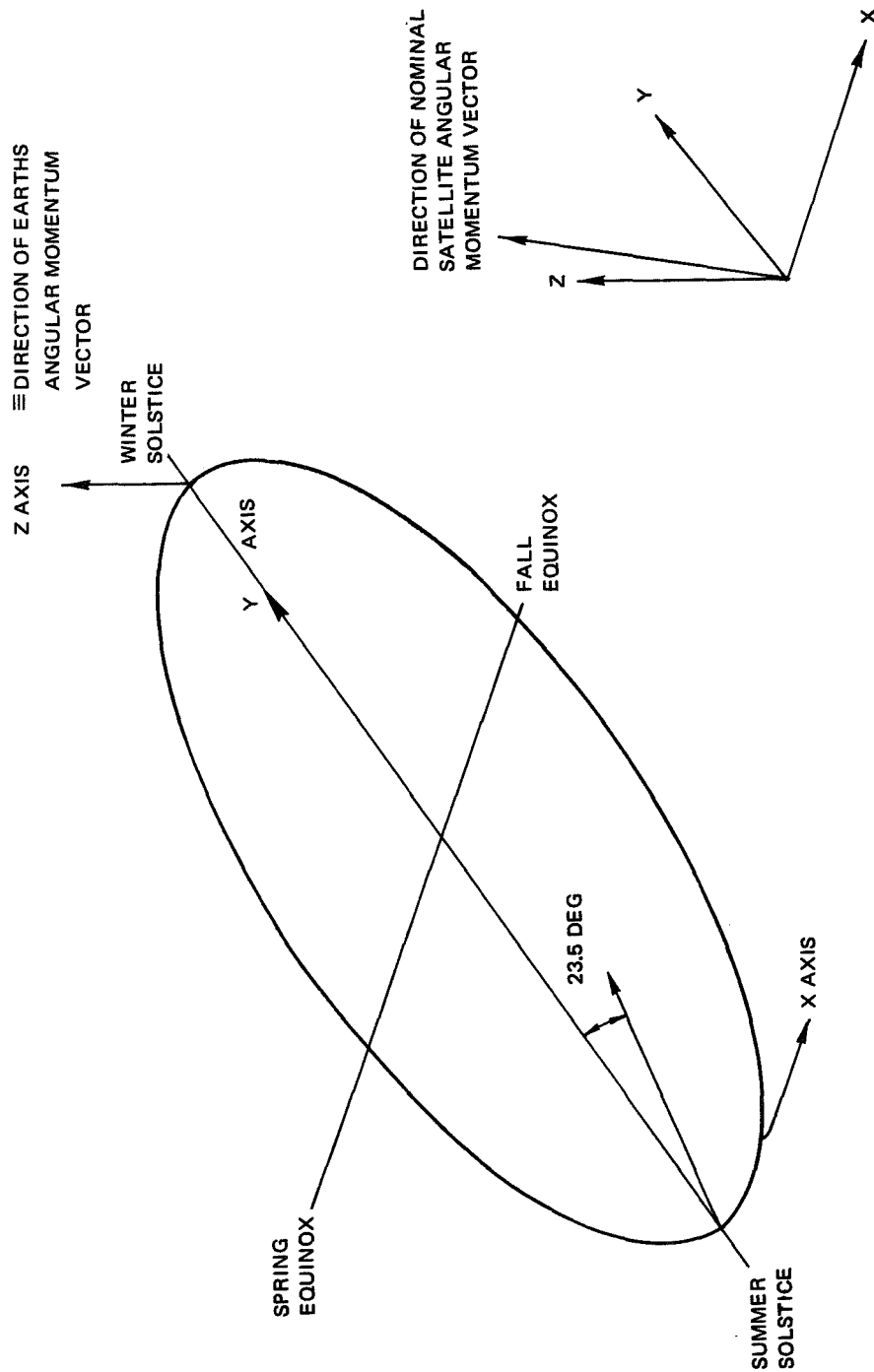


FIGURE 3.3-1 DEFINITION OF SATELLITE ATTITUDE ANGLES

3.4 SIGNIFICANCE OF TELEMETERED PARAMETERS

To properly interpret the telemetered parameters as they relate to solar array performance, it is necessary to understand the interaction of the partial shunt regulator with the solar array. Figure 3.4-1 presents a simplified block diagram of the regulation scheme and a graphical representation of the solar array and its typical operating points. The parameters of significance are as follows:

I_{MB} = Main bus current

V_{MB} = Main bus voltage (29.4 ± 0.2 VDC)

I_{CB} = Control bus current

V_2 = Control bus voltage

V_1 = Unshunted array voltage ($V_1 = V_{MB} - V_2$)

The primary purpose of the partial shunt regulator is to limit the bus to a predetermined voltage; in this case, 29.4 ± 0.2 volts. Regulation is accomplished by sensing the voltage across the main bus, comparing it to a reference voltage, and generating an error signal which is amplified and supplied to the shunt element. This variable impedance shunt element adjusts V_2 such that the sum of V_1 and V_2 equals the main bus regulation set point, 29.4 ± 0.2 volts.

From Figure 3.4-1, it can be seen that changes in I_{CB} are indicative of changes in the current capability of the solar array, assuming the main bus current and the voltage capabilities of the array are held constant. Correspondingly, changes of V_2 are indicative of changes in the voltage capability of the array assuming the current capability is held constant.

By properly interpreting these telemetered parameters, it is possible to determine the array current and the voltage characteristics. It is also possible to construct the entire knee of the I-V curve by detailed investigation of eclipse entrance data. Knee characteristics will be developed in subsequent reports.

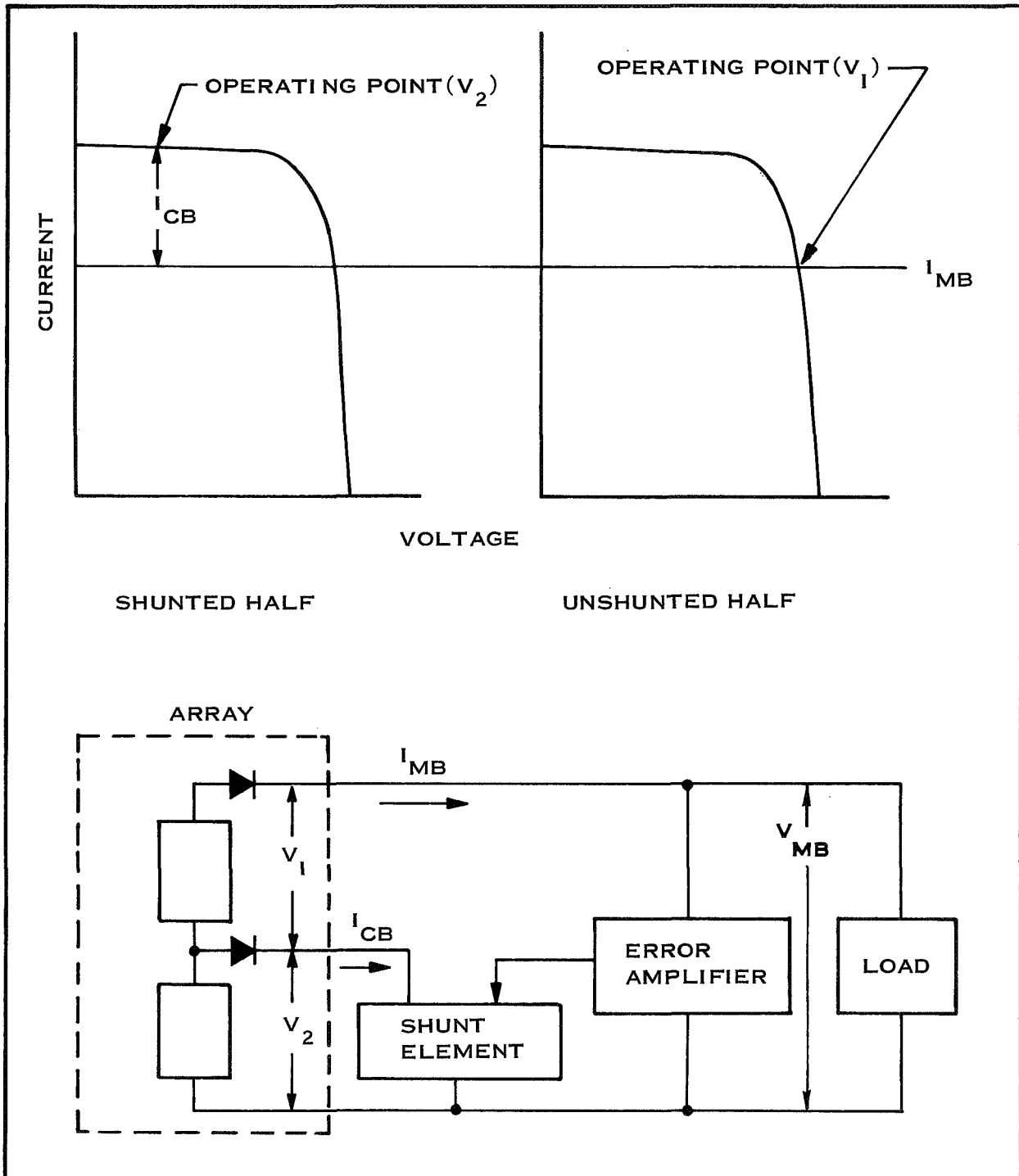


FIGURE 3.4-1 SOLAR ARRAY REGULATOR SCHEMATIC - SIMPLIFIED

3.5 THE EXTRACTION OF DEGRADATION DATA

3.5.1 Basic Method

Stated most simply, the approach followed in this study is the determination of the difference between actual (telemetered), and theoretical undegraded, current and voltage points on the array I-V curve as a function of time on orbit. This difference is used to generate degradation information applicable to a single solar cell on the array.

The theoretical array output is developed on the basis of an assumed typical solar cell manufactured for the IDSCS program. This cell is a 1X2 cm, N on P boron doped silicon cell of 1964 vintage with a base resistivity ranging between 7 and 13 ohm-cm. Figure 3.5-1 presents the I-V characteristic of this cell at 77°F. All cells are shielded by 20 mils of fused silica applied with Dow XR-6-3489 adhesive. A five-parameter (including shunt resistance) single-cell I-V equation is used to develop the total array I-V characteristic considering satellite geometry, sun angle, earth orbit ellipticity and operating temperatures. Temperature dependences (for this vintage of solar cells) are incorporated in each of the cell equation parameters.

Two points on the array I-V curve are effectively monitored by telemetry due to the different loading on the shunted and unshunted halves of the array (reference 3.4). The shunted portion produces a data point close to the short-circuit point and the unshunted portion a point between maximum power and open-circuit voltage. The degradation of these two operating points can thus be tracked vs. time by comparison with the same points on the theoretical array I-V curve.

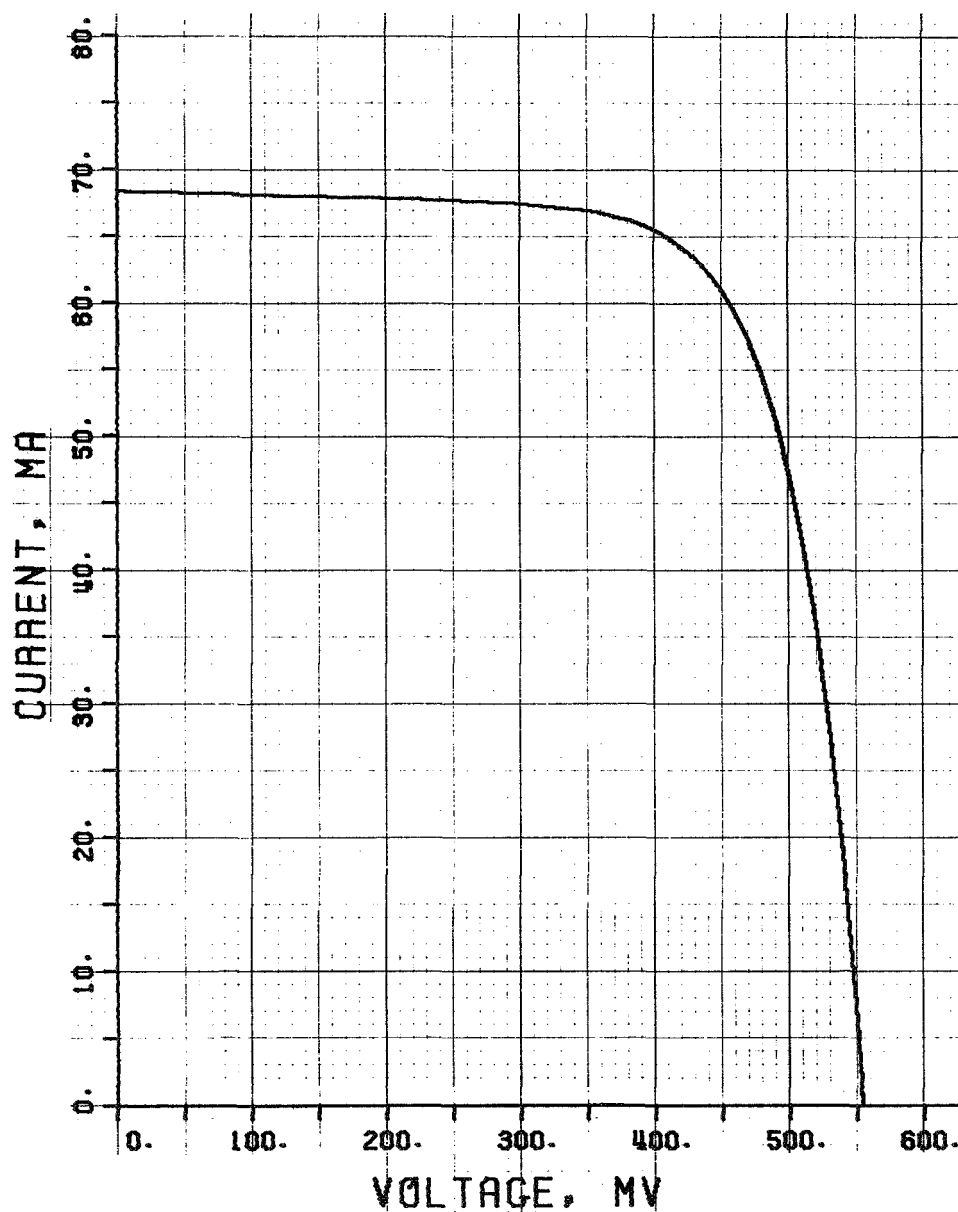


FIGURE 3.5-1 ASSUMED AVERAGE SOLAR CELL I-V CHARACTERISTICS
(BARE NEW CELL AT 25°C (77°F), 1 SUN AMO)

A more sophisticated technique is applied to extract single-cell degradation vs. time of the two interesting parameters, I_{sc} and V_{oc} . An iteration scheme is introduced into the theoretical array I-V computation which finds the corresponding degraded value of the cell I_{sc} which is required to remove the difference between the theoretical and observed array data point near the array short-circuit point. With this degraded value in place, a second iteration is performed which determines the required cell V_{oc} necessary to remove the difference present in the other array data point near the array open-circuit voltage location.

3.5.2 Results to Date

Figures 1-1 and 1-2 (Summary Section) present the collection of satellite degradation curves for cell I_{sc} and V_{oc} as a function of time. These curves summarize the detailed degradation points computer plotted in Section 4.0 for the satellites analyzed to date. The mean deviation of degradation points to an "eyeball" fitted curve appears to be less than 1% which is well within the accuracy of the raw telemetry data points. Least-squares fitted functions and detailed statistical analysis will be performed during a later phase of the contract.

3.5.3 The Detailed Calculations

The assumed basic solar cell equation for forward characteristics is the conventional lumped-parameter expression written* as follows:

$$I = I_L - I_0 \left[\exp \frac{V+IR}{B} - 1 \right] - \frac{V}{P} \quad (1)$$

*Notation and definition of the terms are listed in Appendix A.

This implicit relationship between I and V has been approximated by a semi-iterative explicit expression for I(V):

$$I(V) = I_L - E \exp \frac{R(I_2 + I_3)}{2B} - \frac{V}{P}$$

$$\text{where } I_3 = I_L - E \exp \frac{R I_2}{B}$$

$$I_2 = I_L - E \exp \frac{R I_1}{B}$$

$$I_1 = (I_L - E) \left(\frac{1}{1 + \frac{RE}{B}} \right)$$

$$E = \exp \frac{V' - A}{B}; \quad V' = V \left(1 - \frac{R}{P} \right)$$

$$A = -B \ln I_o$$

The derivation and accuracy of this explicit relation for I(V) is presented in Appendix A; agreement is excellent (better than 0.01%) over 90% of the I-V curve, with a maximum error of .33% as current approaches the open-circuit voltage point.

The assignment of the cell parameters depends on the selected average cell assumed in the makeup of the array. Methods applicable to determining parameters from empirical I-V data are presented in Appendix B. Temperature dependences of the parameters are determined similarly, and analytical functions are finally assigned to each parameter to produce smooth variation with temperature. Appendix C presents the list of functions

and resultant I-V plots in current use on this program. Test cases have indicated that degradation rates of cells are not too sensitive to operating temperature assignments (within "reasonable" excursions) but absolute values and starting points will differ.

Light-generated current, I_L , of a cell has been assumed to vary directly with incident light intensity and with the cosine of the angle between the cell normal and the incident light direction. The satellite array is constructed with 24 planar panels, or "facets", each containing a series string of 76 or 84 submodules, and each submodule containing 4 parallel cells. The light-generated current of each cell on facet j , where $j = 1$ to 24, is thus

$$(I_L)_j = K I_L \cos(n_j, s)$$

where K is an intensity factor and $\cos(n_j, s)$ is the cosine of the angle between the sun direction and the normal to panel j . If the spin axis of the satellite is designated the z axis of a satellite coordinate system and arbitrary (but consistent) x and y axes assigned relative to it, we may write:

$$\begin{aligned} \cos(n_j, s) &= \cos(n_j, x) \cos(s, x) \sin(s, z) \\ &\quad + \cos(n_j, y) \sin(s, x) \sin(s, z) \\ &\quad + \cos(n_j, z) \cos(s, z) \end{aligned}$$

where the $\cos(n_j, x)$, $\cos(n_j, y)$, and $\cos(n_j, z)$ are the direction cosines of the 24 facets, the angle (s, x) a satellite rotation position angle, and (s, z) the angle between the spin-axis and the sun. The direction cosines

for the IDCSP geometry are listed in Table 4.5-1. As the satellite spins around its z-axis (to maintain gyroscopically a "fixed" orientation in space), the power output ripples sinusoidally eight times per rotation as each subsequent facet faces the sun. Since the telemetry data sampling (once every 2 seconds) is not an exact multiple of the spin rate (approximately 2.7 Hz), readout is assumed random on the power ripple. In this analysis, therefore, the angle (x, s) is fixed at 11.24° to provide an approximate ripple-average output level. The angle (z, s) is a telemetered parameter and actual satellite data is used in each theoretical calculation.

The value of the intensity factor, K, is as follows:

$$K = 0.94 (1 + 0.0167255 \cos Q)^2$$

where $Q = S + 0.033444 \sin S$ radians

$$S = 0.017203 (t + t_L) \text{ radians}$$

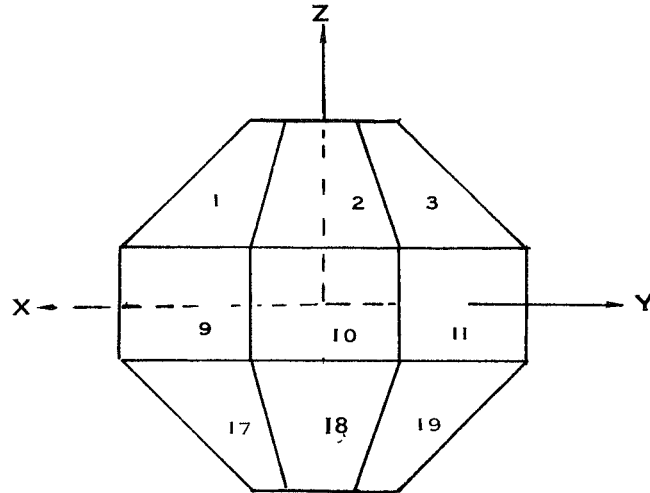
t_L = number of days from Jan 1 to launch date.

The 0.94 factor is due to coverslide and filter losses in the basic solar cell assembly; the time dependent function expresses intensity variation ($\pm 3.5\%$) caused by the slight ellipticity of the earth's orbit around the sun.

The value of I_L is restricted to be positive or zero. The presence of a negative $\cos(s, n_j)$ merely indicates that a facet is in darkness and I_L must be set identically equal to zero. The value of the current output for facet j, I_j , is also restricted to be positive or zero due to the presence of a blocking diode between each cell string and the satellite main bus. This diode also causes a voltage drop of approximately 1 volt in each string.

TABLE 3.5-1

LIST OF DIRECTION COSINES



Facet j	$\cos(n_j, x)$	$\cos(n_j, y)$	$\cos(n_j, z)$	Temp. Zone
1	0.735	0.000	0.680	I
2	0.520	0.520	0.680	
3	0.000	0.735	0.680	
4	-0.520	0.520	0.680	
5	-0.735	0.000	0.680	
6	-0.520	-0.520	0.680	
7	-0.000	-0.735	0.680	
8	0.520	-0.520	0.680	
9	1.000	0.000	0.000	II
10	0.707	0.707	0.000	
11	0.000	1.000	0.000	
12	-0.707	0.707	0.000	
13	-1.000	0.000	0.000	
14	-0.707	-0.707	0.000	
15	0.000	-1.000	0.000	
16	0.707	-0.707	0.000	
17	0.735	0.000	-0.680	III
18	0.520	0.520	-0.680	
19	0.000	0.735	-0.680	
20	-0.520	0.520	-0.680	
21	-0.735	0.000	-0.680	
22	-0.520	-0.520	-0.680	
23	0.000	-0.735	-0.680	
24	0.520	-0.520	-0.680	

The facet angles of the satellite geometry cause a temperature variation between various sets of facets. Due to the high spin rate, the satellite is effectively divided into three temperature zones (with the assigned facet numbers indicated in Table 3.5-1). These zone temperatures are also telemetered parameters and actual values are used to determine cell parameters valid in each of the I_j calculations.

Referring to the previous section on the significance of the telemetered parameters, we obtain different load points on the array I-V characteristic by considering the shunted and unshunted halves separately:

$$V_{UN} = V_{MB} - V_{CB}$$

$$I_{UN} = I_{MB}$$

$$V_{SH} = V_{CB}$$

$$I_{SH} = I_{MB} + I_{CB}$$

The expected undegraded theoretical currents are thus calculated as follows:

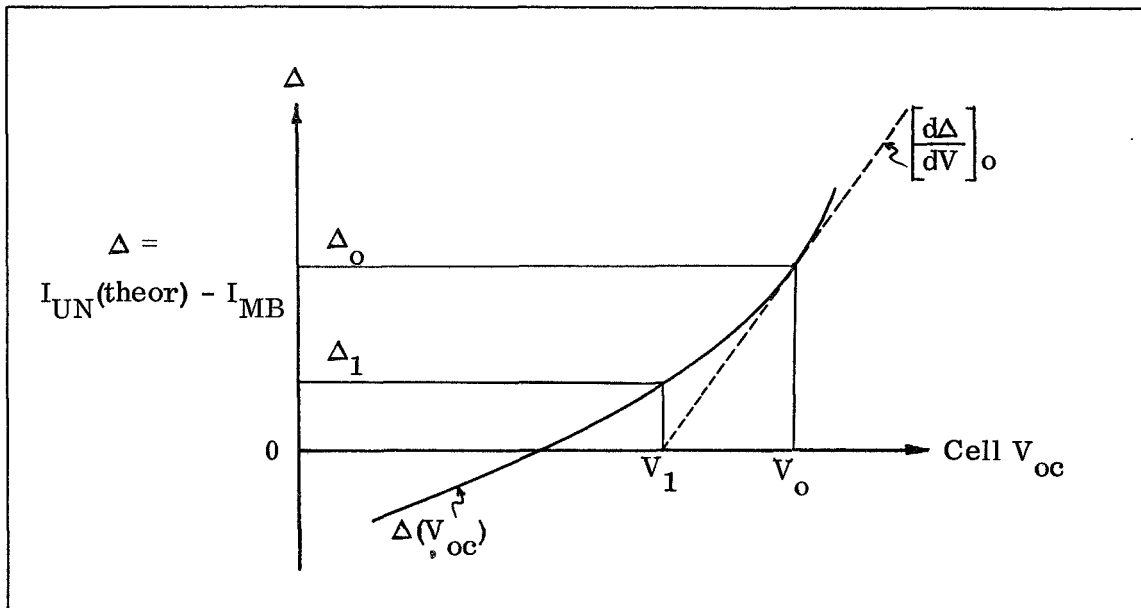
$$\begin{aligned} I_{UN} \text{ (theor.)} &= 4 \sum_{j=1}^8 I_j \left(t, T_1, \frac{V_{UN}}{42} \right) \\ &+ 4 \sum_{j=9}^{16} I_j \left(t, T_2, \frac{V_{UN}}{38} \right) \\ &+ 4 \sum_{j=17}^{24} I_j \left(t, T_3, \frac{V_{UN}}{42} \right) \end{aligned}$$

$$\begin{aligned}
I_{SH} \text{ (theor.)} = & 4 \sum_{j=1}^8 I_j \left(t, T_1, \frac{V_{SH}+1}{42} \right) \\
& + 4 \sum_{j=9}^{16} I_j \left(t, T_2, \frac{V_{SH}+1}{38} \right) \\
& + 4 \sum_{j=17}^{24} I_j \left(t, T_3, \frac{V_{SH}+1}{42} \right)
\end{aligned}$$

The differences between the above theoretical currents and the observed telemetered currents are the most direct degradation outputs of this study. Since $V_{CB} \approx 8$ volts, it is observed that the degradation of the I_{SH} load point must be very close to the degradation of the array short-circuit current point. If no shape changes occur in the array I-V curve, it is further observed that the degradation of V_{UN} which produces the change in the I_{UN} load point must be very close to the degradation of the array open-circuit voltage point.

Of more significance to any degradation analysis is the change in I_{SC} and V_{OC} of a single solar cell, since all ground irradiation tests are made at this level. Iteration algorithms have thus been carried out to determine what factors of initial cell I_{SC} and V_{OC} (at room temperature) must be inserted to remove the differences between theoretical and observed current values. These factors are those plotted in Section 4.

The iteration scheme assumes that the current difference is a linear function of cell I_{SC} or V_{OC} :



The slope of the function $\Delta(V_{OC})$ at Δ_O is determined by a small test variation in V_{OC} at its initial value, V_O . The first, and subsequent, iterative values aimed at reducing $\Delta(V_i)$ to 0 ± 0.001 are calculated as follows:

$$V_i = V_{i-1} - \left[\frac{dV}{d\Delta} \right]_{i-1} \Delta(V_{i-1})$$

In practice, $\Delta(I_{SC})$ was reduced to less than 0 ± 10^{-10} amps within two iterations and $\Delta(V_{OC})$ to less than $0 \pm .0005$ amps within seven. (Note that in both cases Δ is a current difference treated as a dependent function, first of I_{sc} and then of V_{oc}).

DETAILED RESULTS

SECTION 4.0

4.1 DETAILED RESULTS

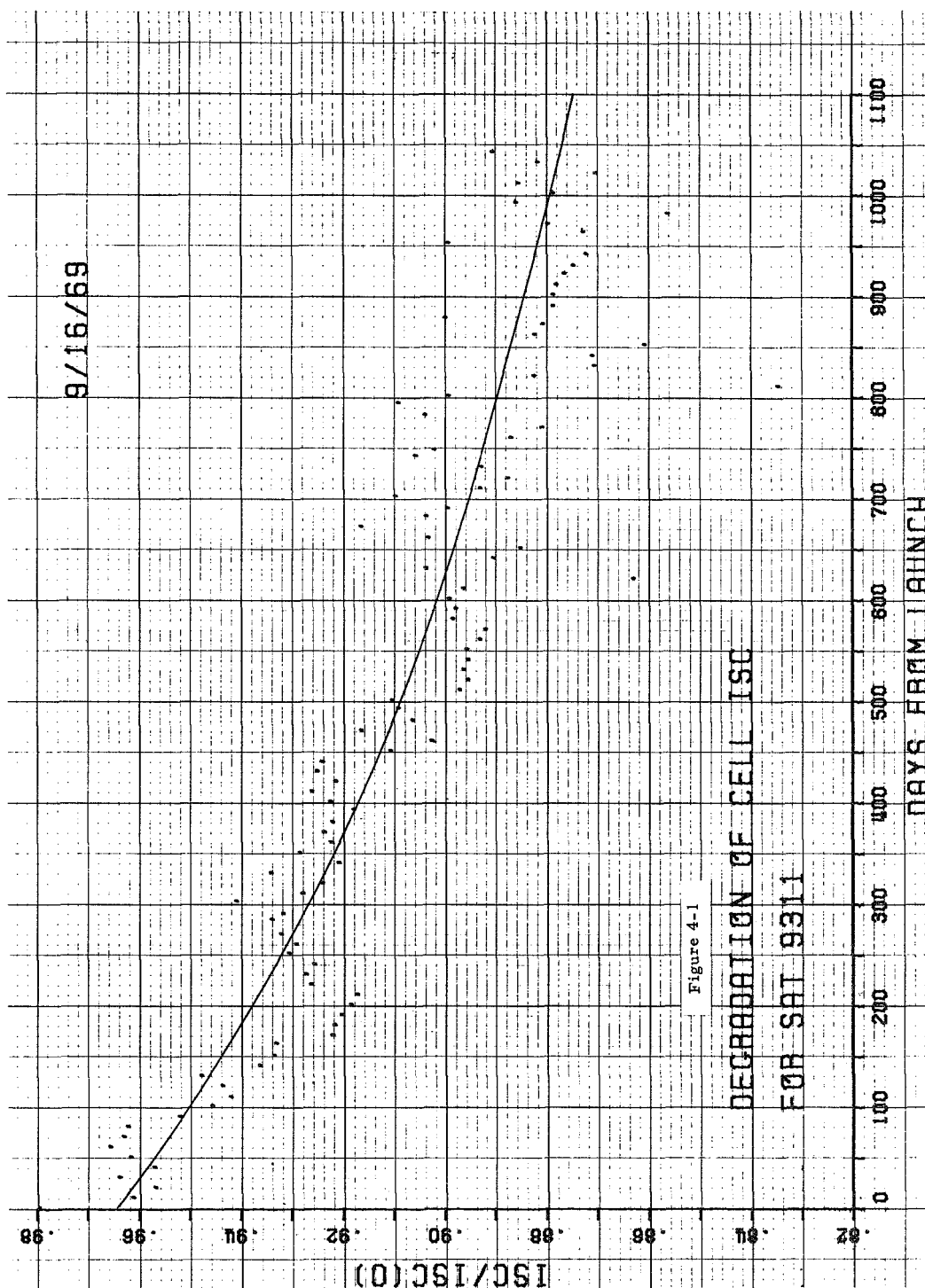
This section is comprised of 14 plots which present the detailed point-by-point degradation information obtained above. Figures 4-1 to 4-7 show cell I_{sc} ratios calculated (generally) every ten days; and Figures 4-8 to 4-14 show the corresponding cell V_{oc} ratios. The basic telemetry data is that of the seven satellites of the first IDSCS payload, launched June 16, 1966.

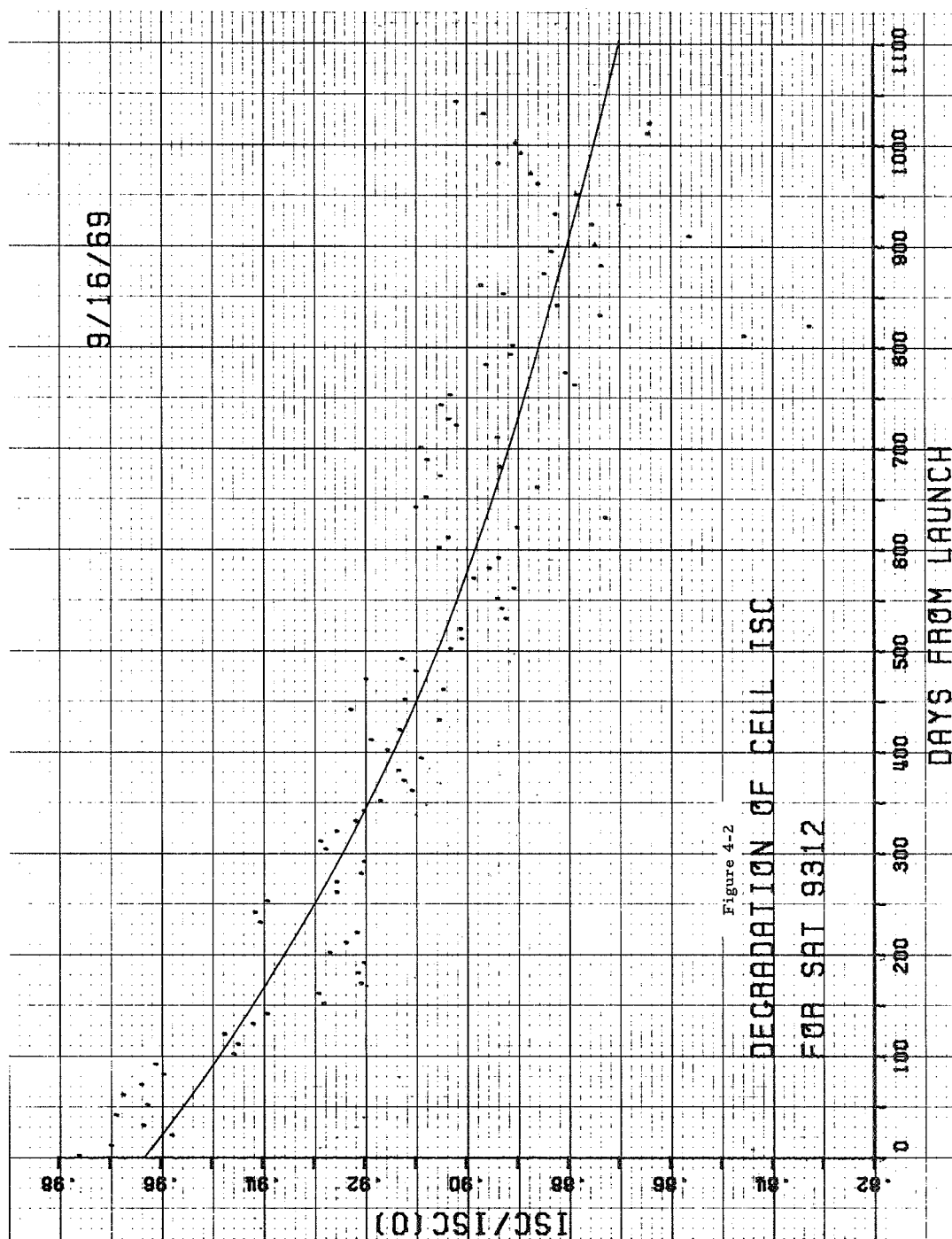
Each graph contains a visually fitted curve which is intended to provide a tentative indication of probable degradation trends. Since the cell quality varies slightly among satellites, the fixed assumed average cell output used in the analysis will produce variations in the initial values (at time zero) of the current and voltage ratios. The collection of tentative curve fits has been normalized (ratio = 1.00 at time = 0) and displayed comparatively in two figures in Section 1.0.

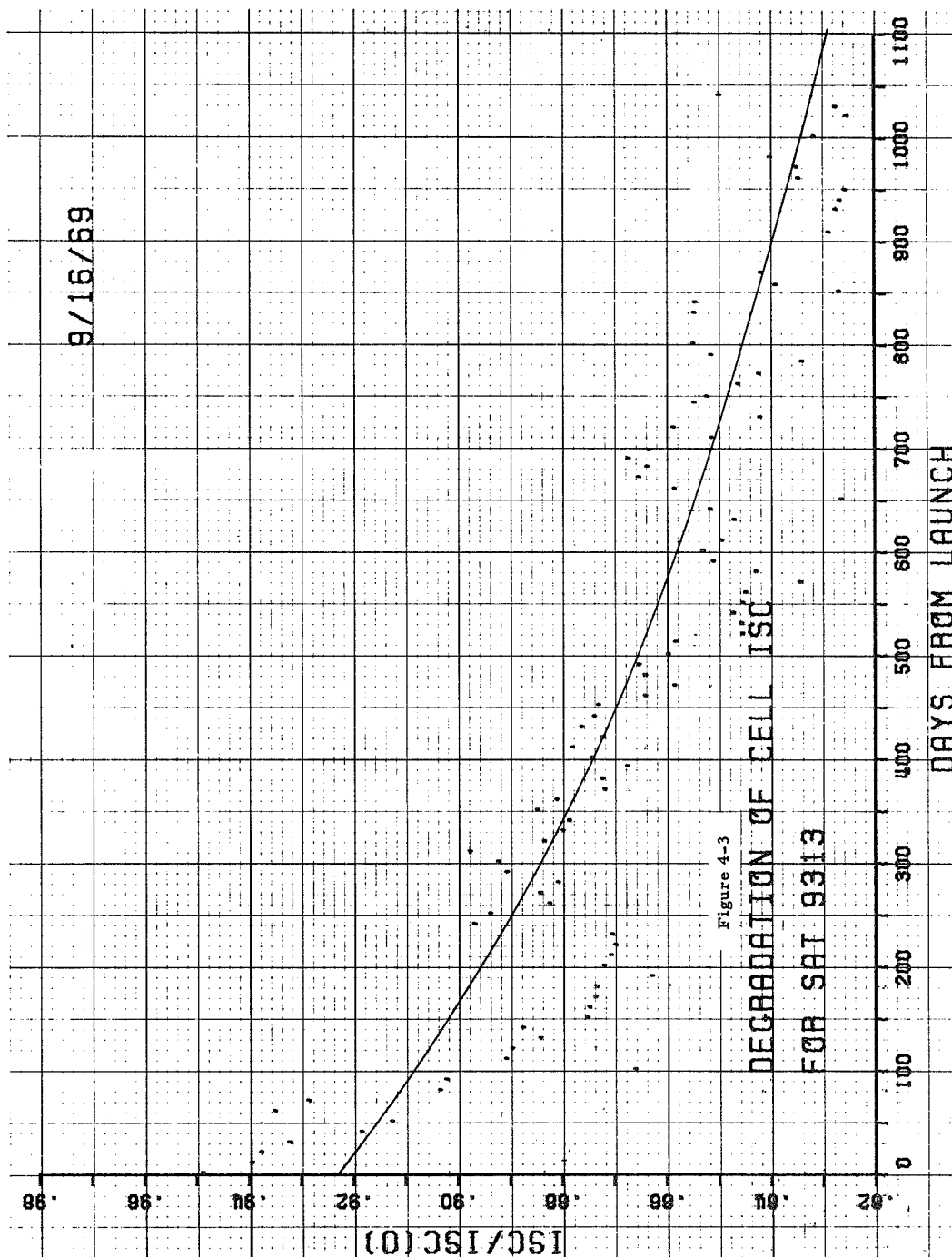
The wide breaks in the data display of satellite No. 9314 (Figure 4-4 and 4-11) are due to internal problems on the satellite; the telemetry system became intermittent after about three months in orbit. Operation is limited to periods of eclipse exit when the transmitter is cold. Transient thermal conditions may account for the observed data scatter.

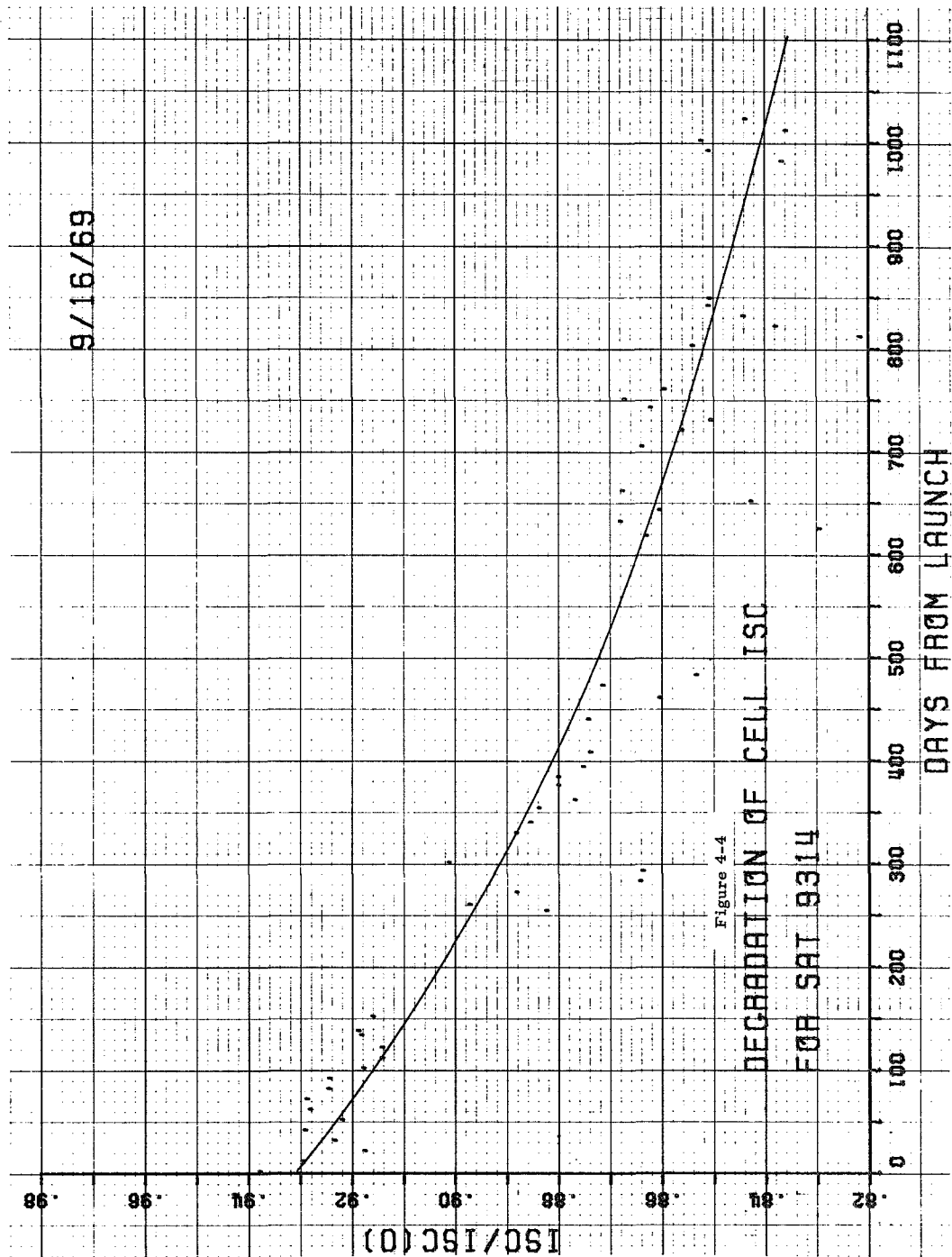
Satellite No. 9316 indicates a degradation rate anomalously greater than the collection of six other first payload satellites (see Figure 1-1). No explanation is currently available for this behavior.

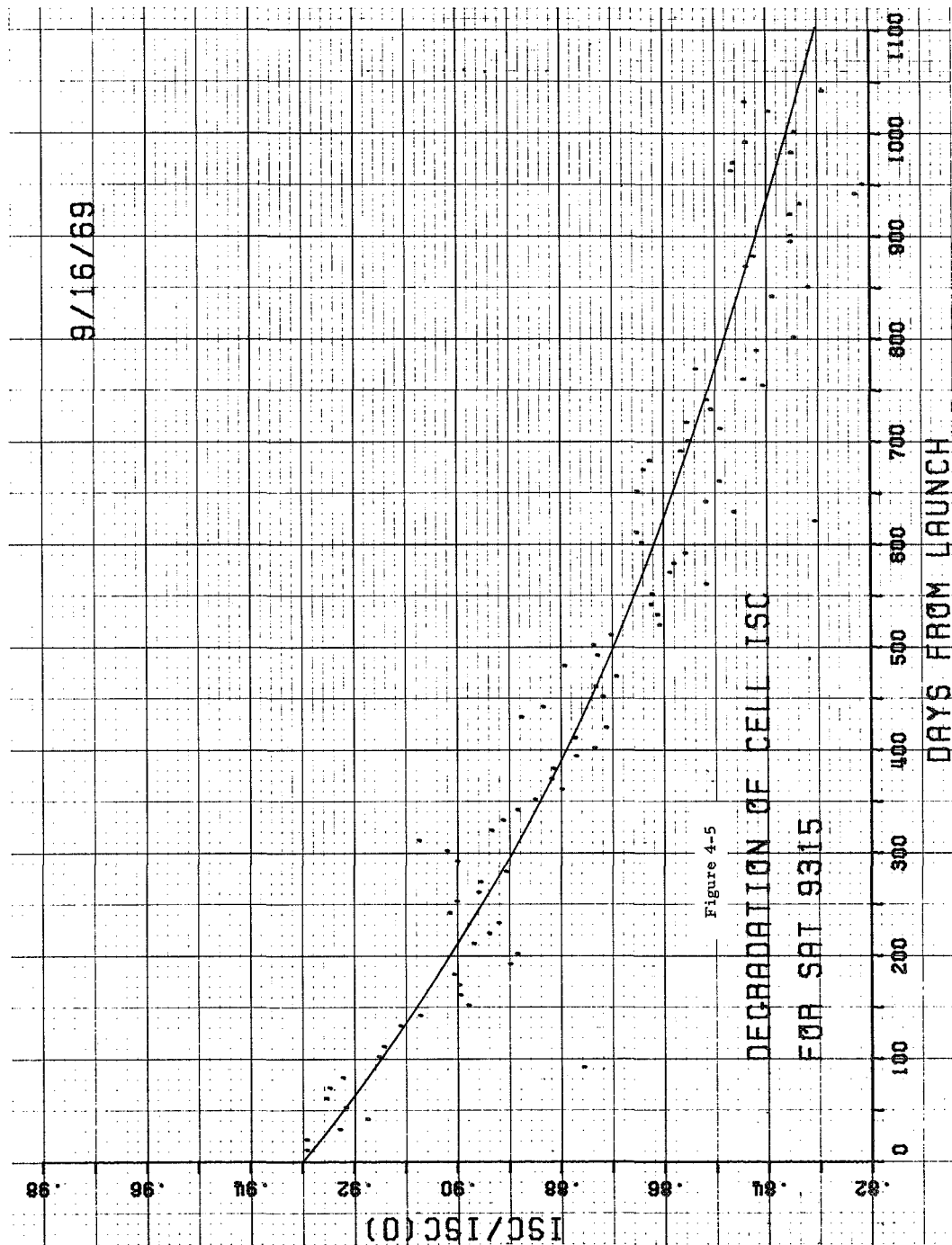
Data points showing large scatter from the fitted curves are presently being examined. Since ten day data was always inputted without regard for whether or not the satellites were in thermal equilibrium after eclipse exit, some of the scatter may be assignable to this fact.

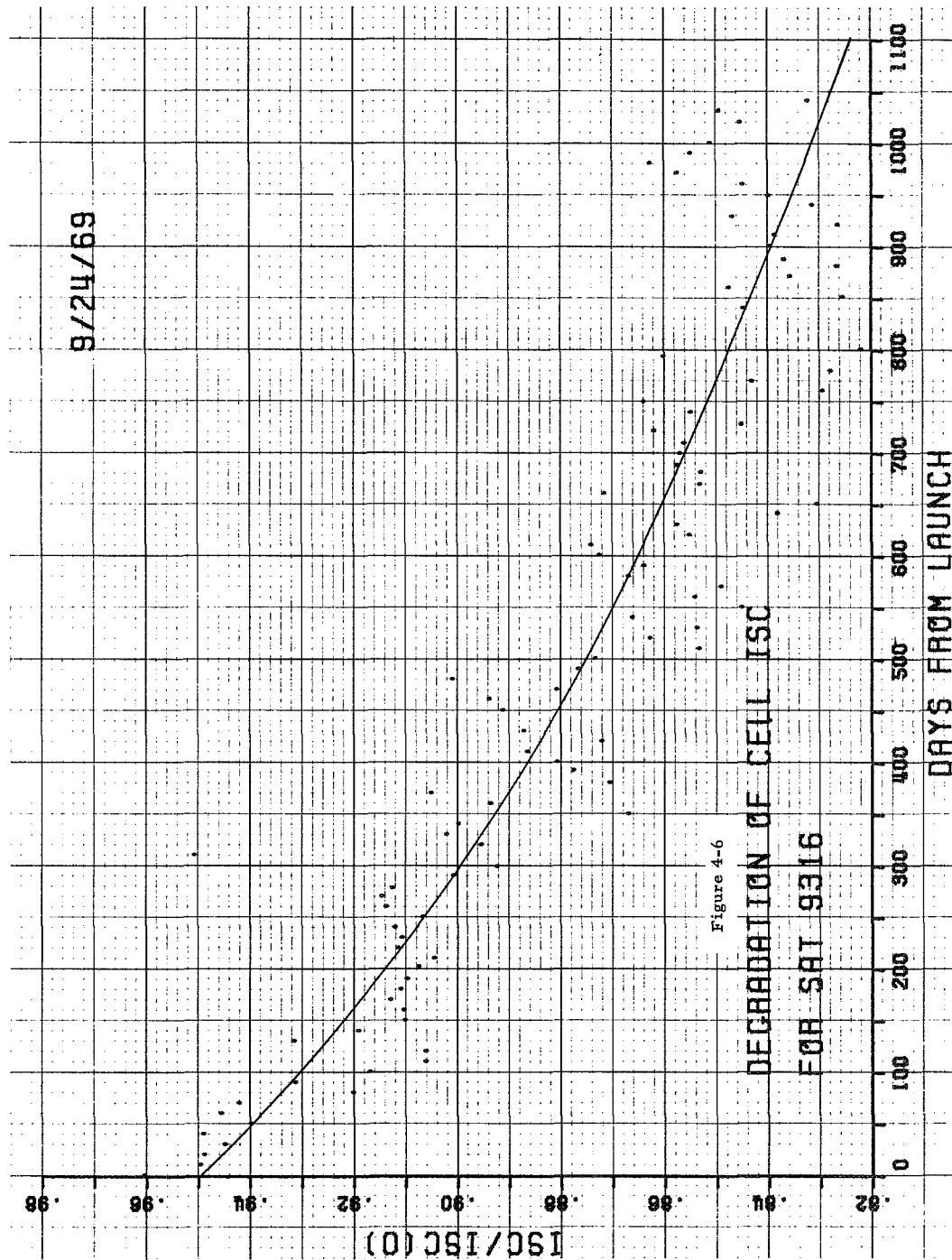


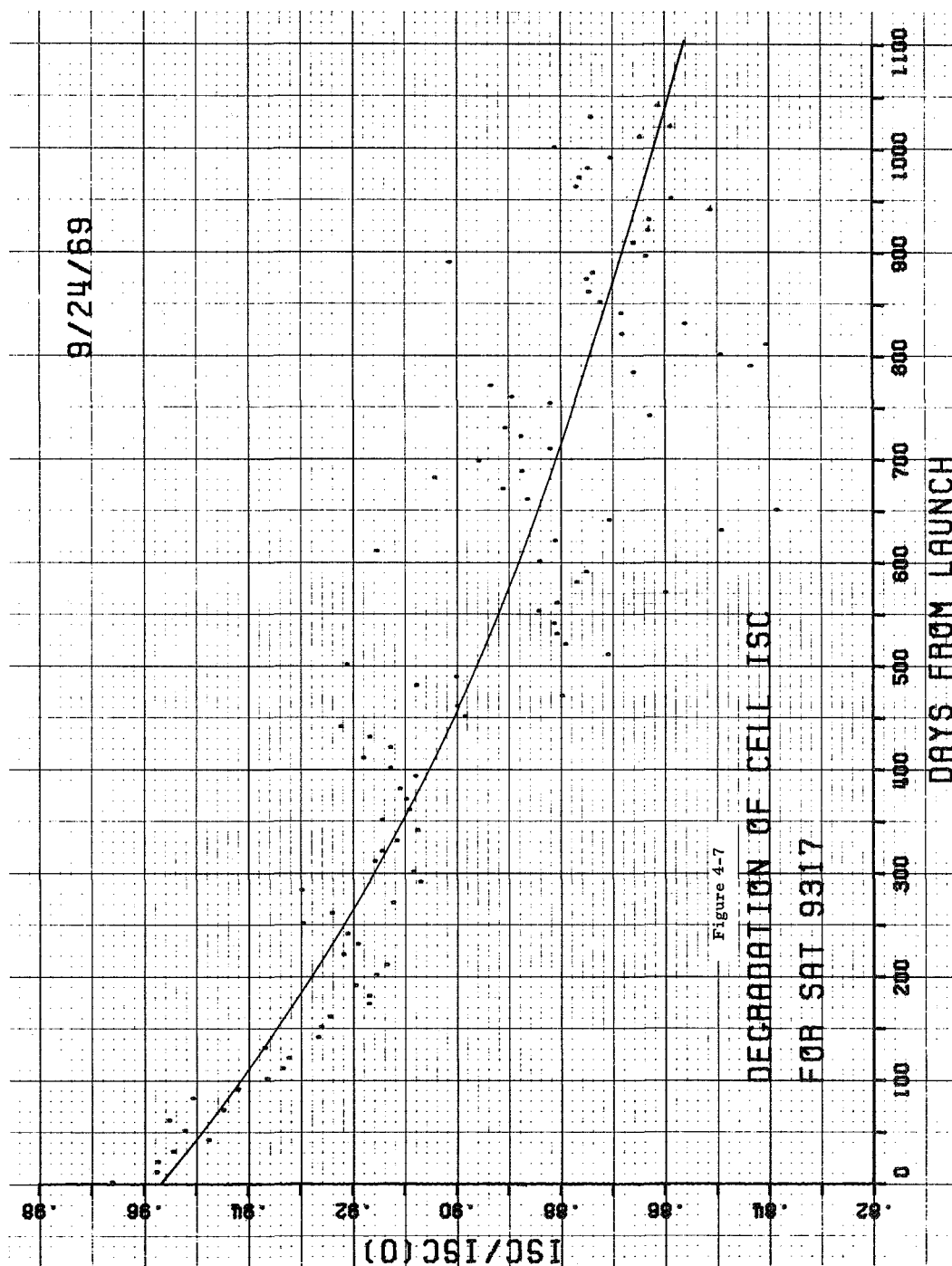


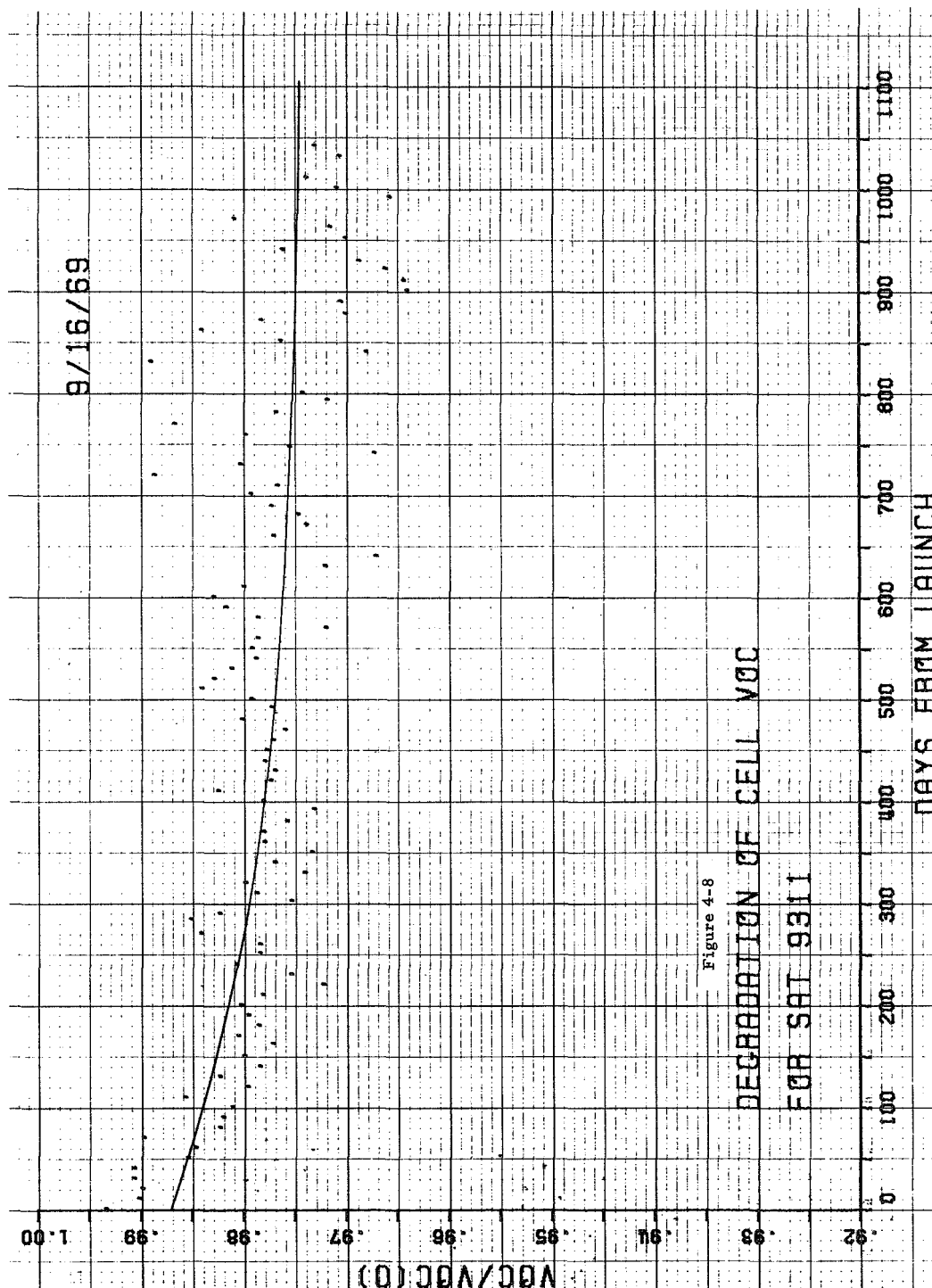


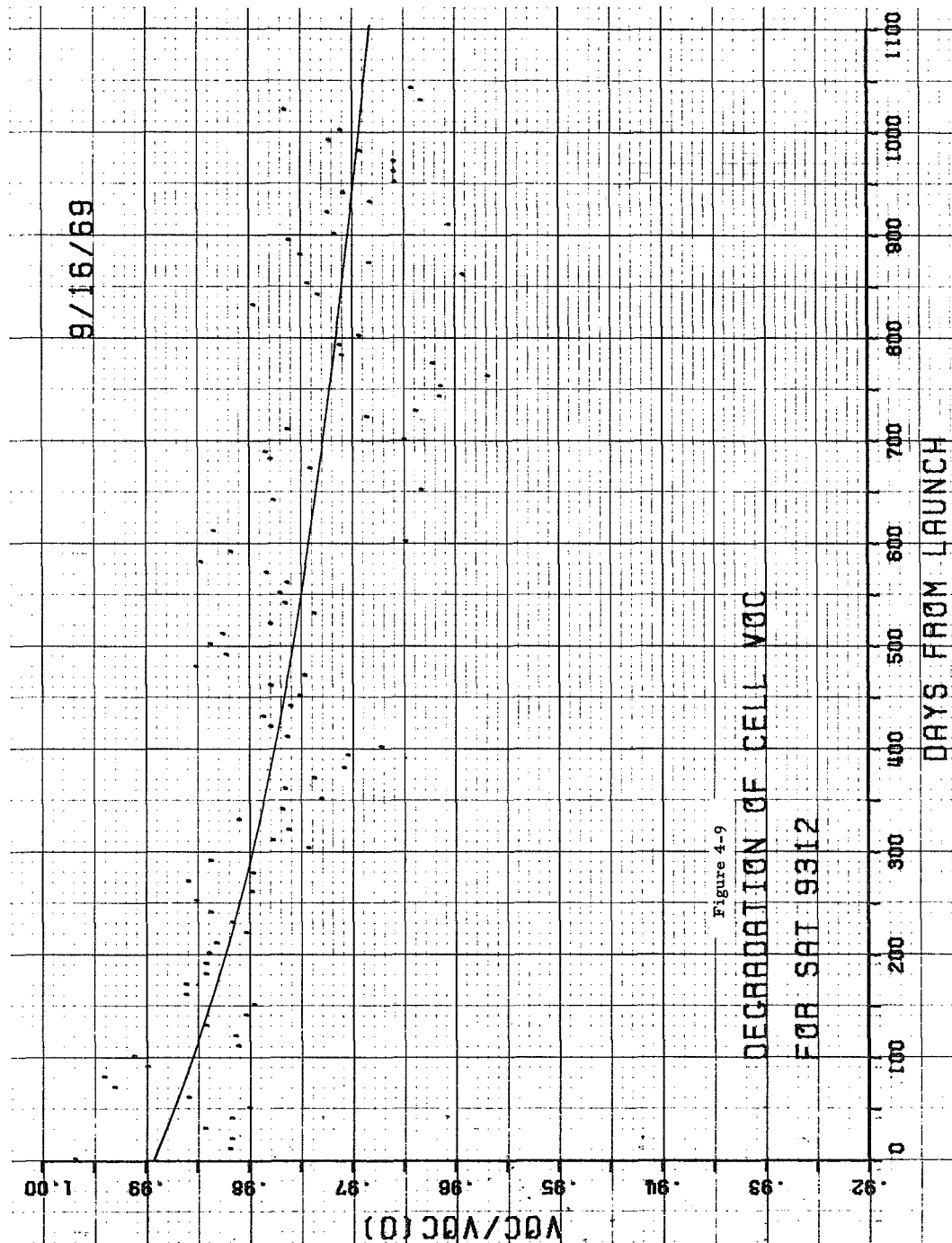


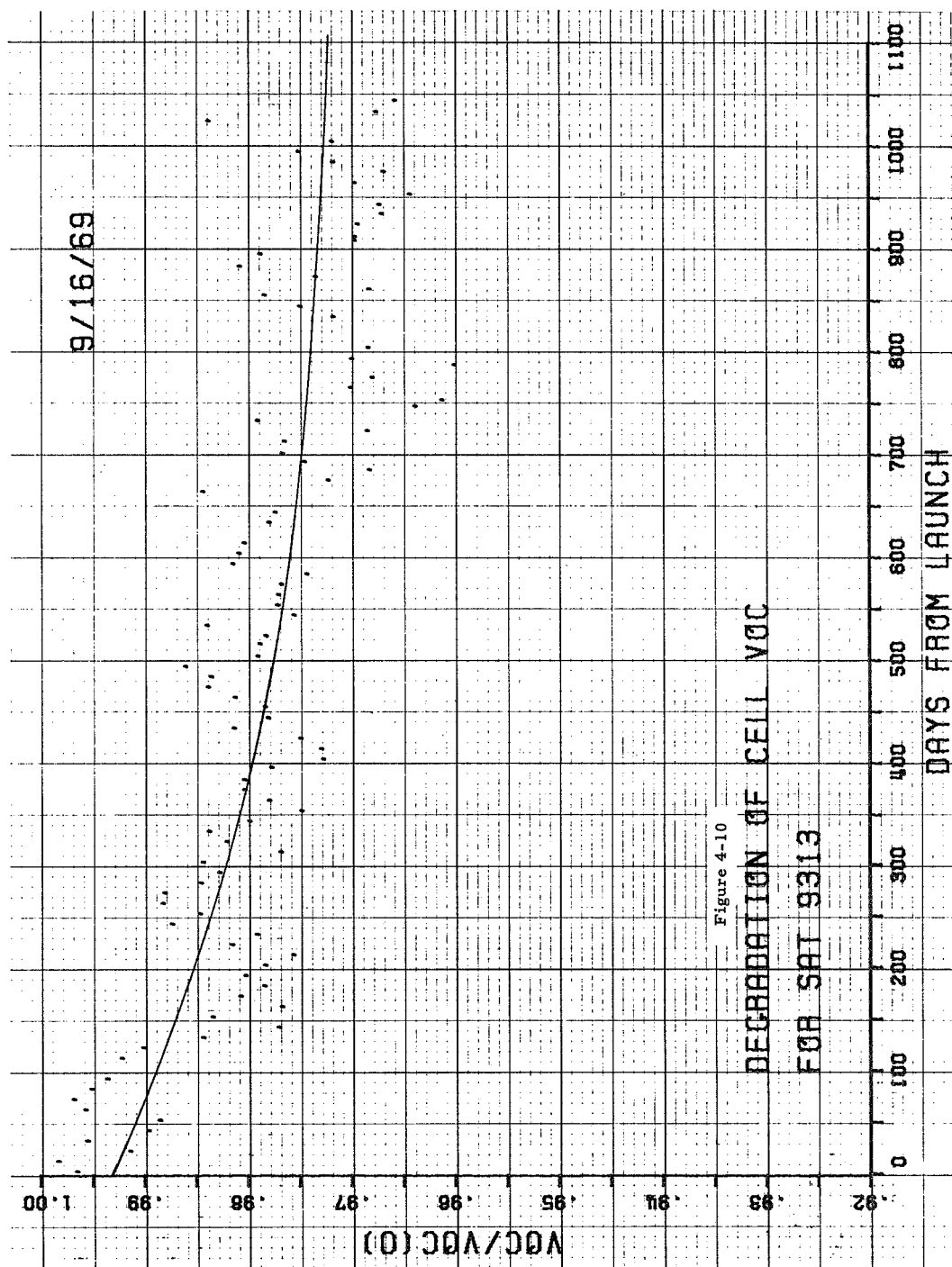


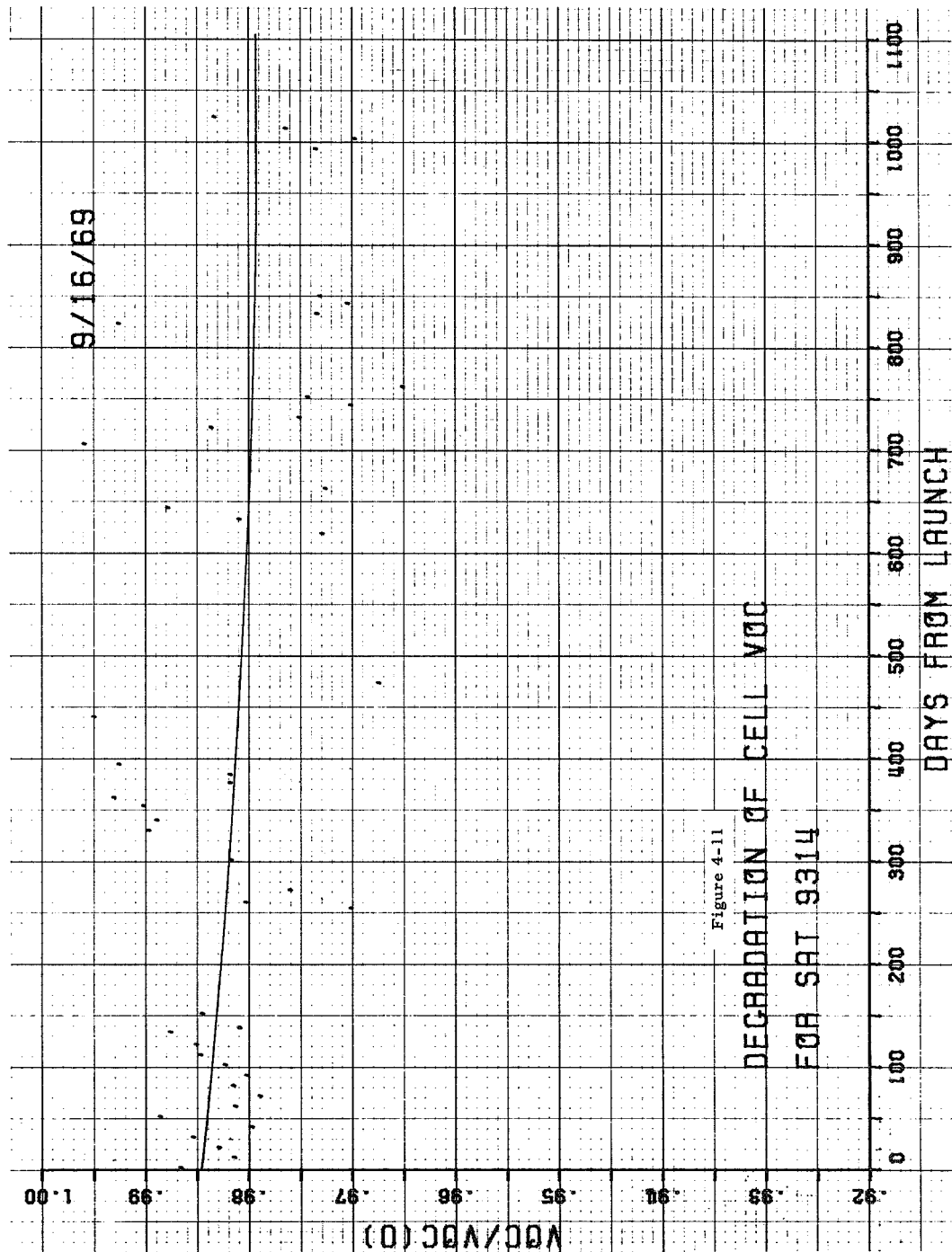


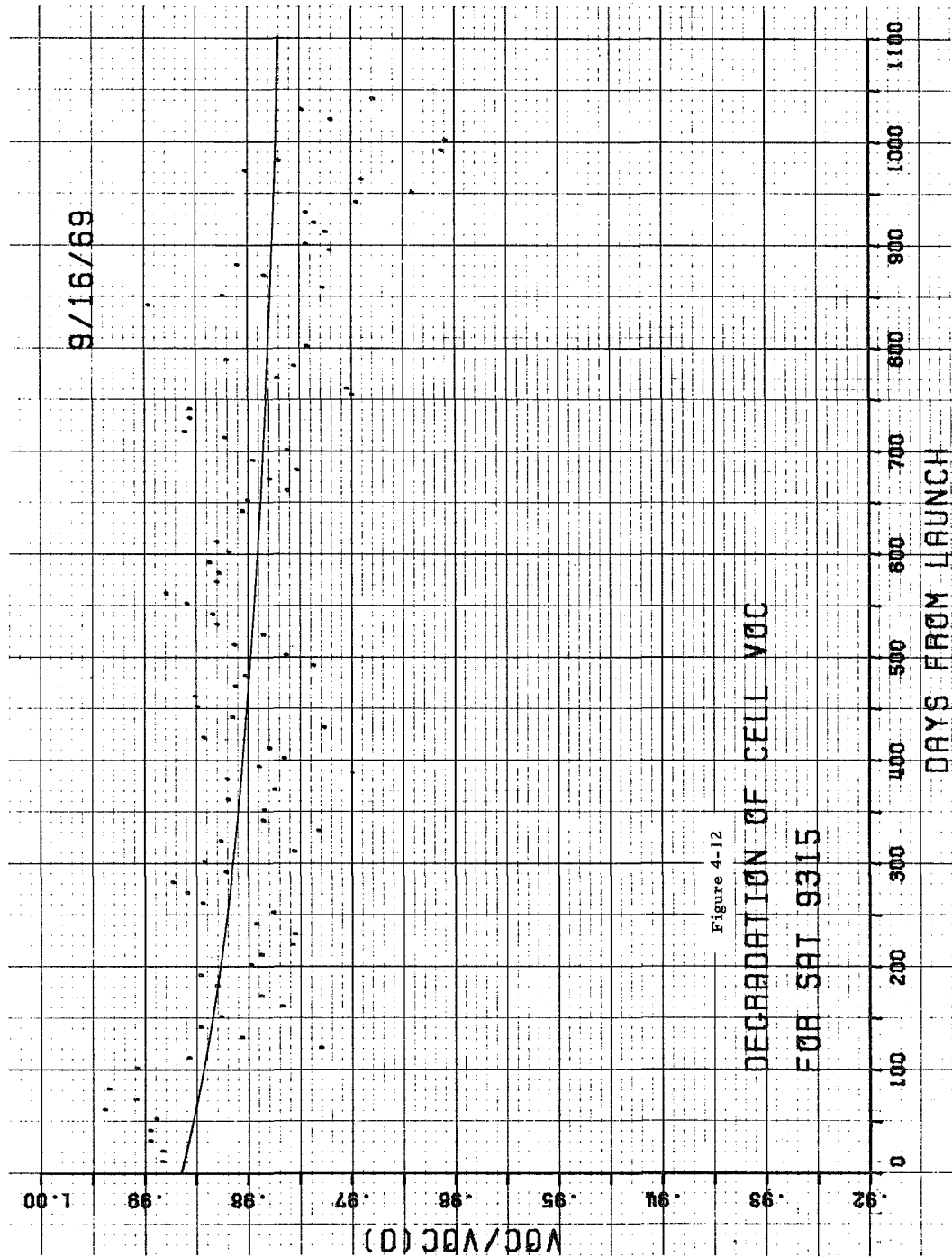


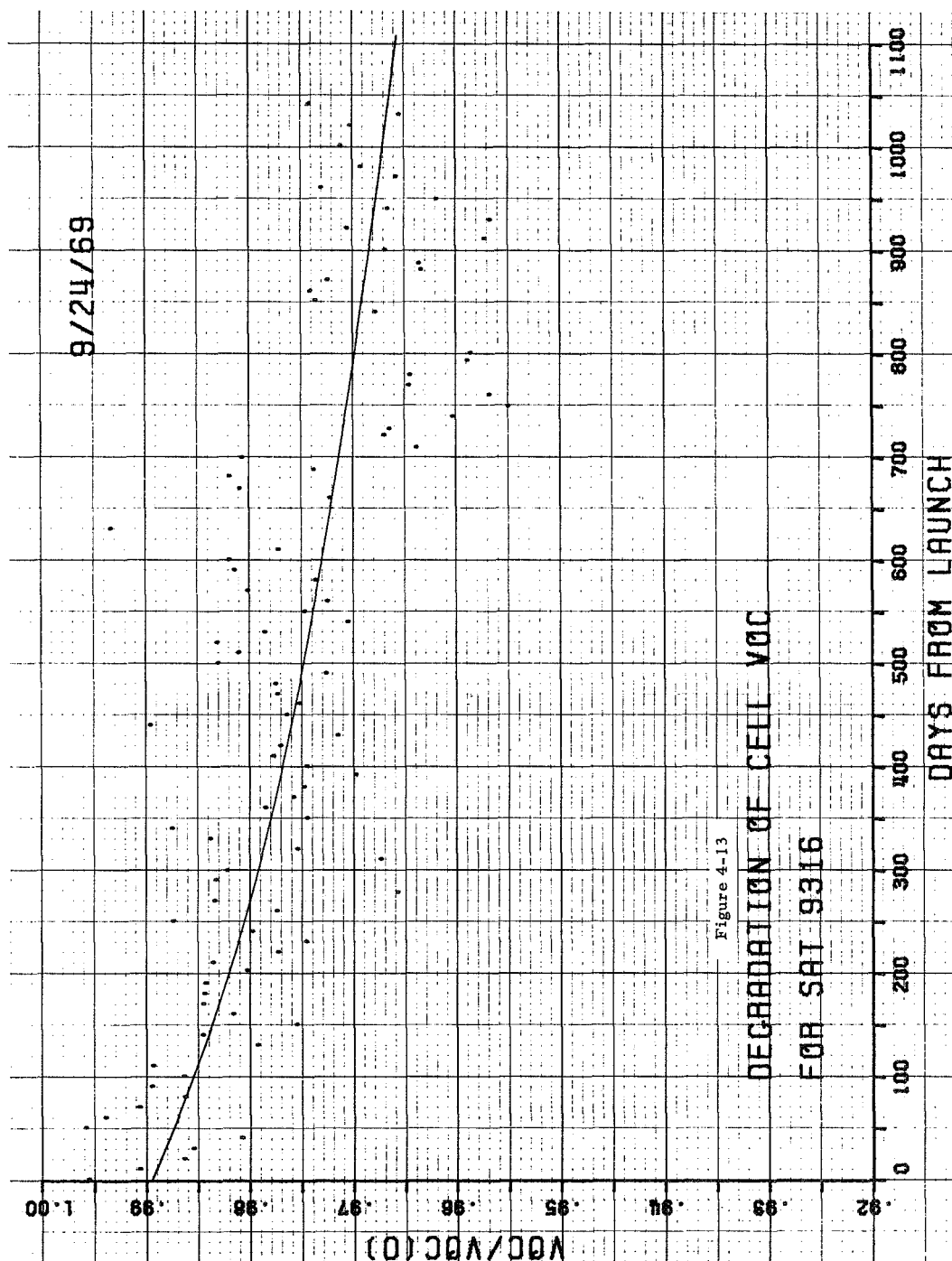


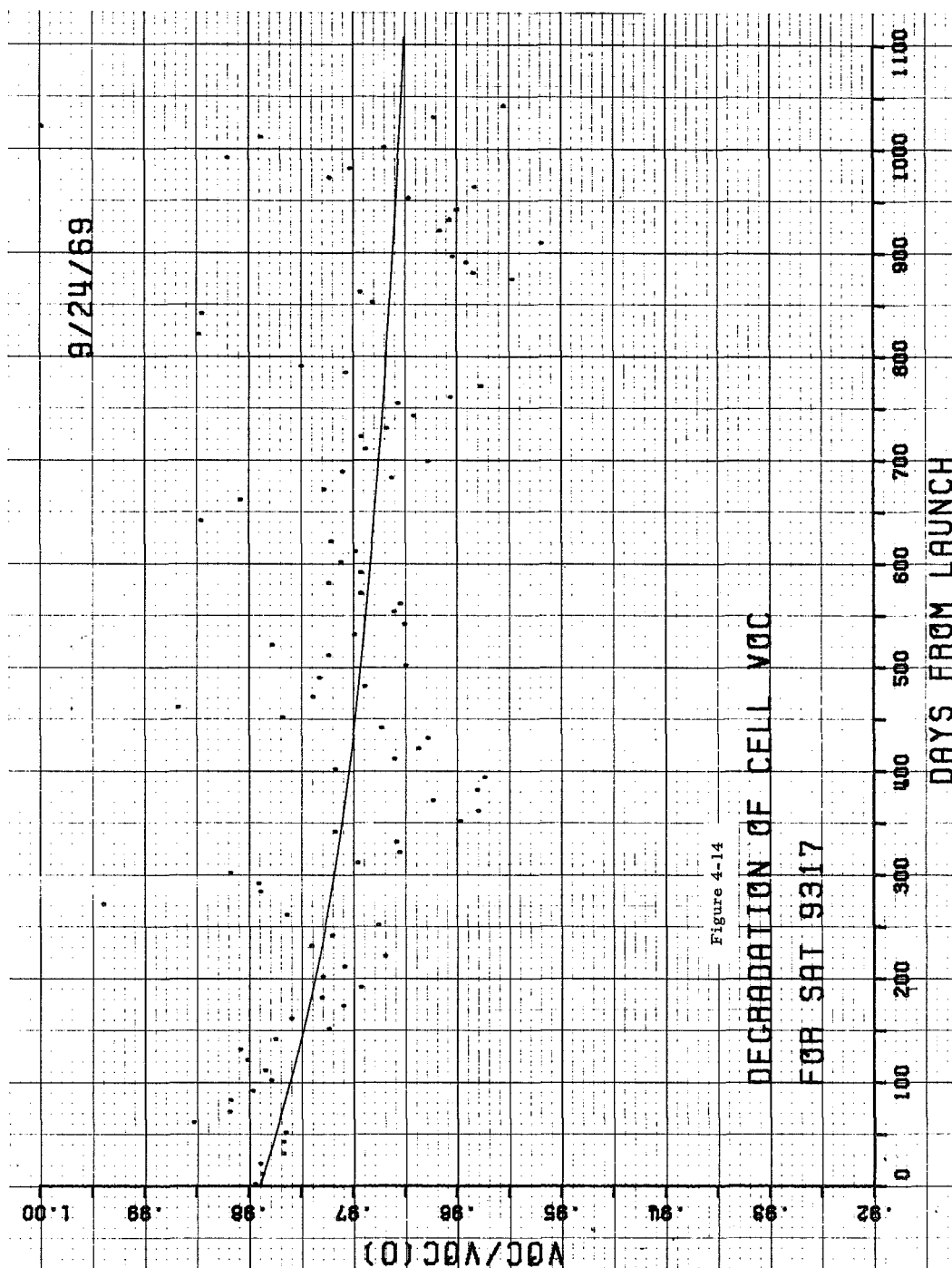












APPENDIX A

DERIVATION AND ACCURACY OF AN EXPLICIT FUNCTION FOR $I(V)$

The assumed basic solar cell equation for forward characteristics is the conventional lumped-parameter version written as follows:

$$I = I_L - I_o \left[\exp \frac{(V + IR)}{B} - 1 \right] - \frac{V}{P} \quad (1)$$

where I = cell current output at voltage V when the cell is illuminated and under resistive load

I_L = light-generated current (assumed approximately proportional to the light intensity incident on the solar cell)

I_o = dark (saturation) current.

$B = \frac{nkT}{q}$, where k is Boltzmann's constant, T the absolute temperature, q the electron charge, and n a dimensionless constant compensating for non-ideal junction behavior ($n=1$ for an ideal diode; $n=2$ when recombination in the space charge region controls the junction current)

R = the lumped series resistance of the cell

P = the lumped parallel (shunt) resistance of the cell.

The substitutions

$$I_o = \exp(-A/B)$$

$$I' = I + \frac{V}{P}$$

produce

$$I' = I_L - \exp \frac{V(1-R/P) - A}{B} \exp \frac{I'R}{B} + I_o.$$

Since $I_o \approx 10^{-7}$, $I_L \gg I_o$, we discard I_o . The exponential containing $I'R$ is expanded to first order:

$$\exp \frac{I'R}{B} \approx 1 + \frac{I'R}{B}$$

and I' rearranged to produce

$$I'_1 = \frac{I_L - E}{1 + \frac{ER}{B}}$$

where $E = \exp \frac{V(1-R/P) - A}{B}$

The second and third iterations are simply

$$I'_2 = I_L - E \exp \frac{I'_1 R}{B}$$

$$I'_3 = I_L - E \exp \frac{I'_2 R}{B} .$$

Observing the effects of typical values of I , R , and B , we find that $(1 + \frac{I'R}{B}) < \exp \frac{I'R}{B}$ and thus I'_1 is greater than the true $I'(V)$. Subsequent effects of this expansion are that $I'_2 < I'(\text{true})$ and $I'_3 > I'(\text{true})$. Advantage is taken of this oscillatory behavior about $I'(\text{true})$ to produce our final iteration:

$$I'_4 = I_L - E \exp \frac{(I'_3 + I'_2) R}{2B}$$

or

$$I(V) \cong I_L - E \exp \frac{(I'_3 + I'_2) R}{2B} - \frac{V}{P}$$

This approximate explicit relation has been compared to solutions of the exact implicit lumped-parameter equation and portions of the computer output are tabulated below. Parameter values are typical of cells applicable to this study.

$$A = 0.6641$$

$$B = 0.0423$$

$$R = 0.4$$

$$P = 367$$

$$I_L = 0.069$$

$$I_O = 1.5194251 \times 10^{-7}$$

<u>V</u>	<u>EXACT I</u>	<u>APPROX.I(V)</u>	<u>% ERROR</u>
0	.06899986	.068999708	-0.000220
0.20	.068422377	.068422225	-0.000222
0.40	.064339857	.064339958	+0.000157
0.45	.056919932	.056924937	+0.00879
0.48	.047510458	.047531384	+0.0440
0.50	.038032126	.038070307	+0.100
0.53	.017842863	.017873693	+0.173
0.55	.000073900	.000074144	+0.331

APPENDIX B

EXTRACTION OF PARAMETERS FROM I-V DATA

Parameters are extracted for two principal reasons: analysis of the parameters, per se, for the purposes of assessing cell quality or change trends due to radiation, temperature, aging, or other environmental exposures; and for the purpose of generating analytical I-V curves to duplicate original empirical curves. The former demands high statistical accuracy and requires computer techniques; the latter is less stringent and may be performed by hand or with the aid of a desk calculator. Both approaches will be discussed but only the simpler algorithms will be detailed in this appendix. The presentation will generally proceed from most simple (least guaranteed accuracy) to most complex (maximum statistical accuracy).

Five parameters (including "lumped" shunt resistance) are considered in each case. For modem cells the presence of the shunt resistance term may not be significant and simplifications will result by letting $P \rightarrow \infty$. If P is very high, normalization of the I-V curve is applicable, ($I_{\text{norm}} = I/I_L$; $V_{\text{norm}} = V/V_{\text{oc}}$). Normalization reduces the number of parameters to be extracted from three to two (assuming $I_L = I_{\text{sc}}$).

Method I: THREE POINTS, TWO SLOPES

Algorithm:

1. Measure the slope of the I-V curve at the short-circuit current point. $\frac{dV}{dI}(V=0) = -P$
2. Measure slope at open-circuit voltage point. Let $\frac{dV}{dI}(I=0) = -m$
3. Let $I_L = I_{\text{sc}}$; obtain V_{oc} ; obtain point near knee (V_k, I_k).
4. Calculate A, B, and R:

$$\text{Let } D = I_L \ln(I_L - I_k - V_k/P) - I_L \ln(I_L - V_{oc}/P) + I_k$$

$$DA = \left[mI_k (V_{oc}/P - I_L) - I_L V_k \right] \ln(I_L - V_{oc}/P) \\ + I_L V_{oc} \ln(I_L - I_k - V_k/P) + I_k V_{oc}$$

$$DB = I_L (V_k - V_{oc}) + mI_k (I_L - V_{oc}/P)$$

$$DR = m(I_L - V_{oc}/P) \left[\ln(I_L - I_k - V_k/P) - \ln(I_L - V_{oc}/P) \right] \\ - V_k + V_{oc}$$

Derivation:

Take the implicit derivative of the exact lumped-parameters cell equation.

Let

$$f = I - I_L + I_o \left(\exp \frac{V + IR}{B} - 1 \right) + \frac{V}{P}$$

$$\frac{dV}{dI} = - \frac{\frac{\partial f}{\partial I}}{\frac{\partial f}{\partial V}} = - \frac{1 + I_o \frac{R}{B} \exp \frac{IR}{B}}{I_o \frac{1}{B} \exp \frac{IR}{B} + \frac{1}{P}}$$

At $V = 0$,

$$I_{sc} = I_L - I_o \exp \frac{I_{sc} R}{B} + I_o$$

$$\frac{dV}{dI} (V = 0) = - \frac{1 + \frac{R}{B} (I_L + I_o - I_{sc})}{\frac{1}{B} (I_L + I_o - I_{sc}) + \frac{1}{P}} \approx -P \quad (1)$$

since the term in parentheses $\approx 10^{-7} - 10^{-8}$.

Similarly,

$$\frac{dV}{dI} (I = 0) = - \frac{I + \frac{R}{B}(I_L - \frac{V_{oc}}{P})}{\frac{1}{P} + \frac{1}{B}(I_L - \frac{V_{oc}}{P})} \equiv -m$$

Multiplying numerator and denominator by B, we can simplify by dropping third order terms. This is justified because measurements of the slope at this point are difficult to make with high accuracy.

$$I_L \approx 0.07 \text{ to } 0.14$$

$$B \approx 0.04$$

$$RI_L \approx 0.02 \text{ to } 0.07$$

$$V_{oc}/P \approx 0.0014 \text{ to } 0.0002$$

$$RV_{oc}/P \approx 0.0004 \text{ to } 0.0001$$

$$B/P \approx 0.0001 \text{ to } 0.00001$$

Eliminating the lowest two terms only, we obtain

$$B + RI_L \approx m (I_L - V_{oc}/P) \quad (2)$$

Substituting $A = -B \ln I_o$ in the cell equation at $I = 0$, we obtain

$$A + B \ln (I_L - \frac{V_{oc}}{P}) = V_{oc}. \quad (3)$$

Finally, for some point near the knee, (V_k, I_k) , we evaluate the general cell equation and drop the very small term, I_o , which stands alone:

$$A + B \ln(I_L - I_k - \frac{V_k}{P}) - I_k R = V_k. \quad (4)$$

Equations 2, 3 and 4 constitute three relations in the three unknowns, A, B, and R. Using substitutions or determinants, we proceed to the explicit expressions listed in Step 4 of the algorithm.

METHOD II: FOUR POINTS, ONE SLOPE

Algorithm:

1. Measure slope at I_{sc} .

$$\frac{dV}{dI} (V = 0) = -P$$

2. Let $I_L = I_{sc}$; Obtain three points on the I-V curve, preferably two above and below the knee, and one at or near V_{oc} .

3. Calculate A, B, and R;

$$\begin{aligned} \text{Let } D = & (I_1 - I_3) \ln(I_L - I_2 - V_2/P) \\ & + (I_2 - I_1) \ln(I_L - I_3 - V_3/P) \\ & + (I_3 - I_2) \ln(I_L - I_1 - V_1/P) \end{aligned}$$

$$\begin{aligned} DA = & (V_3 I_1 - V_1 I_3) \ln(I_L - I_2 - V_2/P) \\ & + (V_1 I_2 - V_2 I_1) \ln(I_L - I_3 - V_3/P) \\ & + (V_2 I_3 - V_3 I_2) \ln(I_L - I_1 - V_1/P) \end{aligned}$$

$$DB = (I_1 - I_3)V_2 + (I_2 - I_1)V_3 + (I_3 - I_2)V_1$$

$$\begin{aligned} DR = & (V_3 - V_1) \ln(I_L - I_2 - V_2/P) \\ & + (V_1 - V_2) \ln(I_L - I_3 - V_3/P) \\ & + (V_2 - V_3) \ln(I_L - I_1 - V_1/P). \end{aligned}$$

Derivation:

The derivative at $V = 0$ to obtain P was derived under Method I above. Substituting $A = -B \ln I_0$ in the cell equation and three values of (V, I) we rearrange and produce 3 equations in the three unknowns A, B, and R.

METHOD III: PSEUDO LEAST-SQUARES METHOD

Algorithm:

1. Measure slope at I_{sc} .

$$\frac{dV}{dI}(V=0) = -P$$

2. Let $I_L = I_{sc}$; obtain N points on the I-V curve, (V_n, I_n) . Form Q groups of three different points each. The number of possible combinations of N points taken 3 at a time is:

$$Q = \frac{N!}{6(N-3)!}$$

3. Calculate A_q , B_q , and R_q for each group; $q = 1$ to Q .
4. Using the approximate explicit expression for $I(V)$ derived in Appendix A, for each group calculate S_q , the sum of the squares of the deviations of the N data points from the analytical curve generated with the parameters A_q , B_q , and R_q :

$$S_q = \sum_{n=1}^N \left[I_n - I_q(V_n) \right]^2$$

5. Determine the minimum S_q by examination, and obtain the corresponding combination of A, B, and R used in group q. These values will be the "best" parameters derivable by this method.

METHOD IV: TRUE LEAST-SQUARES METHOD

Algorithm:

1. Obtain N points on the I-V curve, (V_n, I_n) .
2. Obtain trial values of the five cell parameters, P_i , from one of the above methods, or by "educated guess". (e. g., let $P_1 = I_L$, $P_2 = A$, etc.)

3. Let $F_n(I_n, V_n, P_i) = I_n - I(V_n, P_i)$

It is desired to adjust the P_i such that

$$\sum_{n=1}^N F_n^2$$

is a minimum. Let $P'_i = P_i + \Delta P_i$ be such an adjustment. Expand each of the corresponding F'_n about their initial values:

$$F'_n = F_n + \frac{\partial F_n}{\partial P_i} \Delta P_i = \epsilon$$

Obtain the $N \times 5$ matrix, H , made up of the $\partial F_n / \partial P_i$. This may be accomplished by evaluation of the functional derivatives or by the approximate method of ratioing the difference in F_n (caused by a variation in some P_i) to the difference in P_i .

4. Let ϵ , F_n , and ΔP_i be 1×5 matrices. Then

$$\epsilon = F_n = H \Delta P_i$$

$$\sum_{n=1}^N (F'_n)^2 = \epsilon^T \epsilon$$

We desire the minimum $\epsilon^T \epsilon$, or

$$\frac{\partial}{\partial P_i} (\epsilon^T \epsilon) = 0$$

Hence,

$$(F_n + H \Delta P_i)^T (F_n + H \Delta P_i) = 0$$

or

$$H^T (F_n + H \Delta P_i) = H^T F_n + H^T H \Delta P_i = 0$$

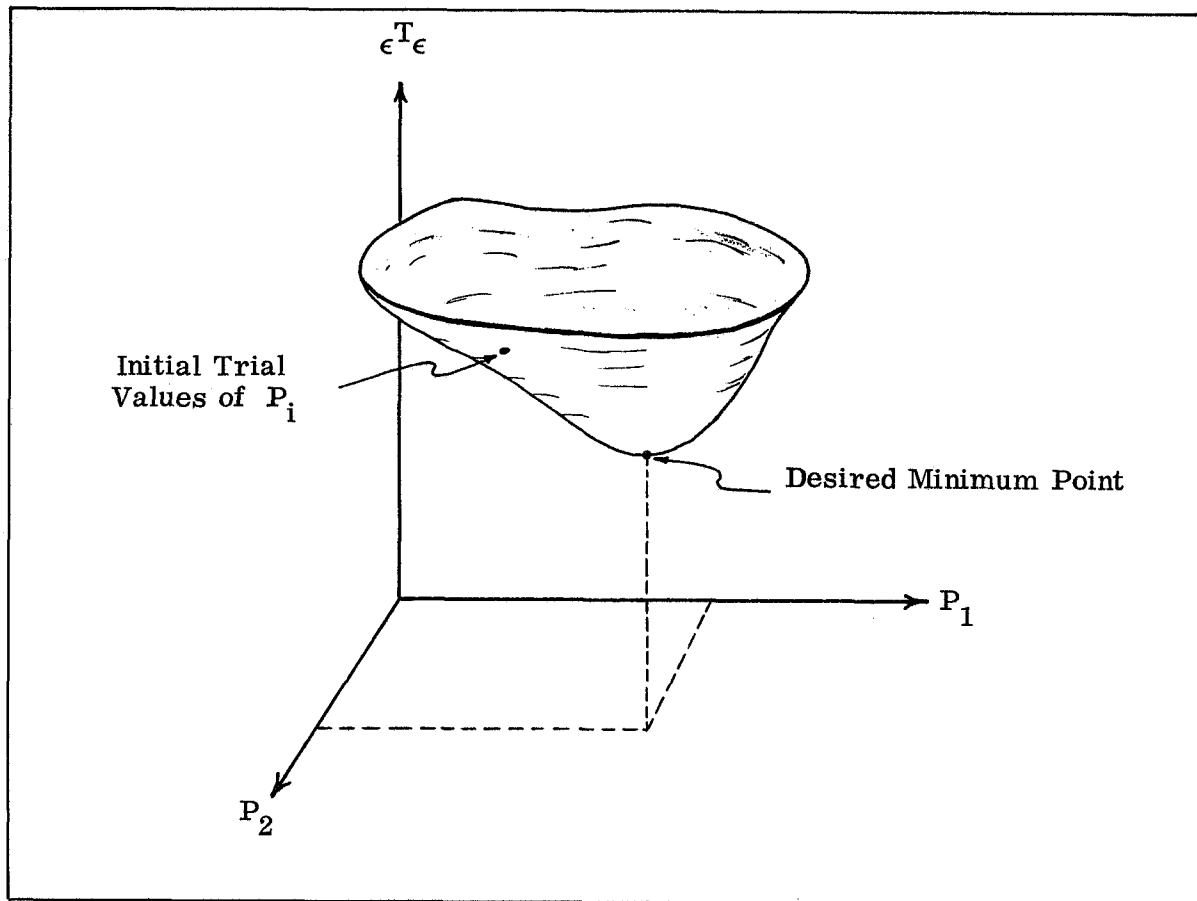
Solving for the ΔP_i matrix, the following calculation must be carried out:

$$\Delta P_i = - (H^T H)^{-1} H^T F_n.$$

5. Calculate P'_i and test $\epsilon^T \epsilon$.
6. Repeat steps 3, 4, and 5 above until $\epsilon^T \epsilon$ converges to a stable minimum value.

Derivation:

The sum of the squares of the deviations between the data points and the curve $I(V_n, P_i)$ may be visualized as a surface in six-dimensional space:



Since $\epsilon^T \epsilon$ is the sum of squared quantities, it is always positive or zero. Any incorrect initial trial set of parameters will always produce a point on the surface above the desired minimum point. The convergence to the minimum point proceeds in a manner analogous to the 2-dimensional iteration scheme described at the end of Section 3.5 for the determination of cell I_{sc} and V_{oc} . The slope of the surface along a path which is the shortest distance to the minimum point is determined; the surface along that path is considered linear, and subsequent iterations aim at reaching the minimum point.

The possibility always exists, when dealing with non-linear functions, of producing anomalous values of the P_i . This phenomenon occurs when "local" minima are present on the $\epsilon^T \epsilon$ surface and when the initial trial parameter set just happens to land near one of them. When the resultant P_i are obviously anomalous, the problem should be rerun with a different set of trial parameters.

APPENDIX C

APPENDIX C

TEMPERATURE DEPENDENCE OF THE PARAMETERS

Tentative temperature functions have been assigned to each parameter on the basis of trends shown in Reynard's^{*} 1965 data. With the absence of the raw (not redrawn) laboratory I-V curves, and an operational least-squares parameter fitting program, a number of simplifying assumptions have been made at this time:

- a. Temperature trends of each parameter have been assumed monotonic, smooth, and generally "well behaved."
- b. The constant, n , defined in Appendix A, has been treated as a true constant (even though some evidence exists that it varies at temperature extremes); hence, $B \propto T$ on an absolute temperature scale.
- c. Normal light intensity values have been assumed: 1 sun or less.
- d. The lumped-parameter solar cell equation has been assumed (c.f. Appendix A, Eqn. 1); solving for I_L at $V =$ produces

$$I_L = I_{sc} + \exp \frac{I_{sc} R - A}{B} - \exp \left(\frac{-A}{B} \right).$$

^{*}D. L. Reynard, Proton and Electron Irradiation of N/P Silicon Solar Cells, Contract No. AF04(647)-787, Lockheed Report No. LMSC 3-56-65-4, 12 April 1965, Figure 26

It is observed that any difference between I_L and I_{sc} is produced by the dissipative series-resistance term only. In the Reynard data, the worst-case fitted values of R produce a difference of less than 0.1 ma between I_L and I_{sc} at 200°F. This small difference justifies the use of the slope at I_{sc} as a means of determining the shunt resistance, P (see derivation in Appendix B). Hence,

$$-\frac{dV}{dI} (V=0) = P$$

- e. The variations in I_{sc} and V_{oc} with temperature have been assumed exactly linear. The rates of change are based on the Reynard cell data.
- f. The theoretical temperature dependence of I_o has not been used. Since the parameter A has been defined to replace I_o ,

$$A = -B \ln I_o,$$

its temperature dependence is derived from a combination of the other parameters.

- g. The measured and fitted temperature variations of P and R have been tentatively expressed by simplified first-order equations.

The assigned temperature variations of the five parameters, expressed as functions of parameters extracted at temperature T_o , are as follows (all temperatures are $^{\circ}\text{F}$):

$$B(T) = B(T_o) \frac{T + 460}{T_o + 460}$$

$$V_{oc}(T) = V_{oc}(T_o) \frac{0.6387 - 0.00129 T}{0.6387 - 0.00129 T_o}$$

$$I_{sc}(T) = I_{sc}(T_o) \frac{0.0663 + 0.00002941 T}{0.0663 + 0.00002941 T_o}$$

$$P(T) = P(T_o) \frac{V_{oc}(T) I_{sc}(T_o)}{V_{oc}(T_o) I_{sc}(T)} \exp \left[.00153 (T_o - T) \right]$$

$$R(T) = R(T_o) \frac{V_{oc}(T) I_{sc}(T_o)}{V_{oc}(T_o) I_{sc}(T)} \exp \left[-.00153 (T_o - T) \right]$$

$$A(T) = V_{oc}(T) - B(T) \ln \left[I_{sc}(T) - \frac{V_{oc}(T)}{P(T)} \right]$$

$$I_L(T) = I_{sc}(T) + \exp \left[\frac{I_{sc}(T) R(T)}{B(T)} - 1 \right] \exp \left[- \frac{A(T)}{B(T)} \right]$$

A family of curves based on these functions is plotted in Figure C-1. The assumed initial parameters are averaged from 12 I-V curves supplied by Heliotek in 1964 for the IDSCS array:

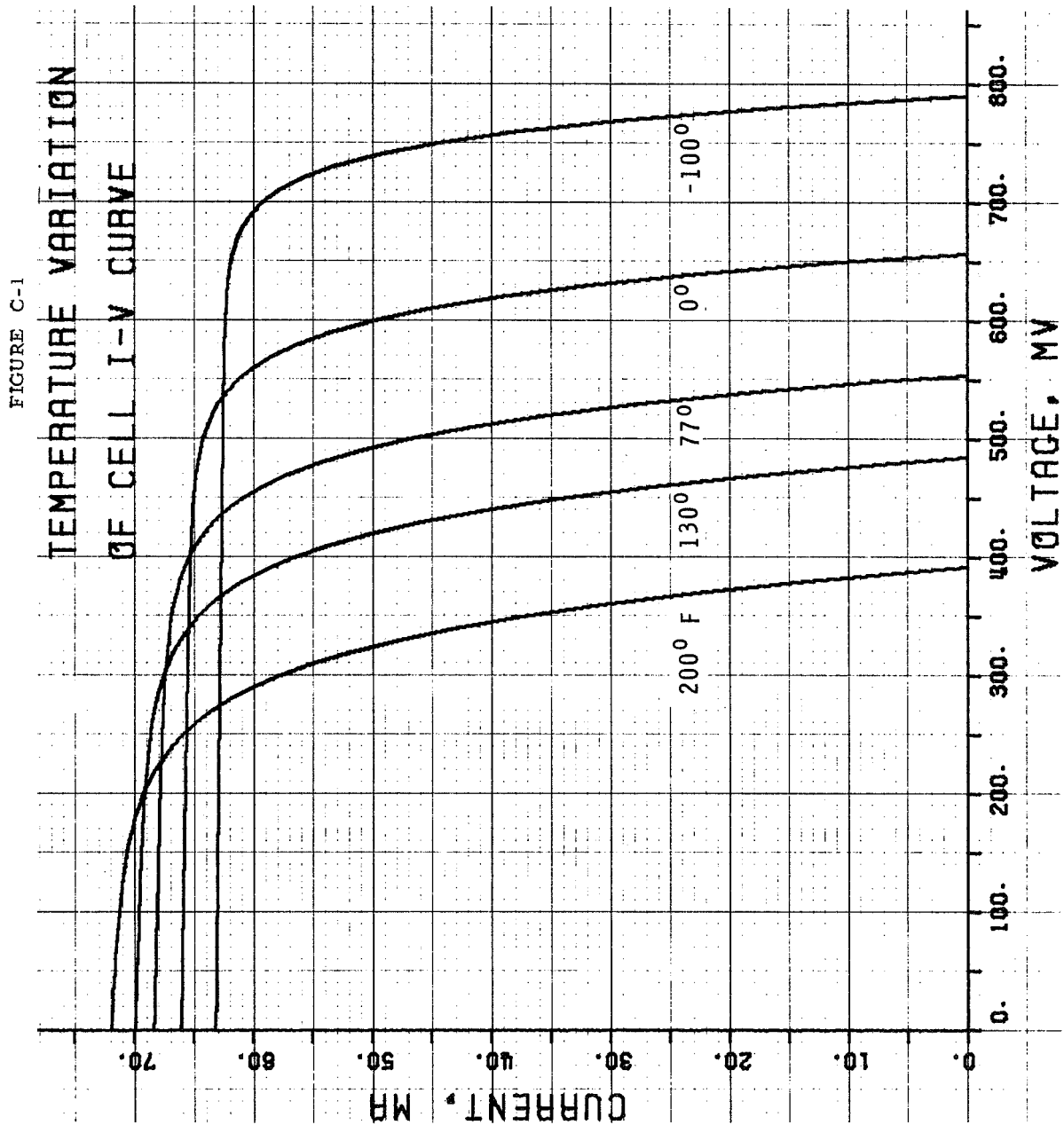
$$B = 0.0423 \qquad T_o = 82.4^{\circ}\text{F}$$

$$V_{oc} = 0.548167$$

$$I_{sc} = 0.0685083$$

$$P = 370.5$$

$$R = 0.10$$



APPENDIX D

APPENDIX D

DEGRADATION ANALYSIS COMPUTER PROGRAM

Basic Design Criteria

The following criteria were considered as a design basis for the program:

1. Easy modification to data structure to allow efficient updating as data are accumulated.
2. Easy development of hard copies of digitized flight data.
3. Block structure for versatility, maximum options in outputting level, and allowance for easy modification and expansion as the contract matures.
4. Rapid and efficient access to allow quick development.

With these criteria in mind, a time-shared computer system was chosen as the facility through which the analysis would be carried out.

Program Description

The flow chart in Figure D-1 shows the implementation of the analysis described in 3.5.

Input Elements

There are three different types of input elements to the program:

1. Elements common to all satellites under consideration which include average solar cell equation parameters, the direction

cosines which define the satellite geometry, the number of cells and their electrical combination comprising the total satellite solar array. As these elements are common, they are included as part of the analysis program.

2. Elements unique to each satellite are the flight data and the satellite number. The flight data needed in the program include:
 - a. Days from launch
 - b. Sun Angle
 - c. Main bus voltage
 - d. Main bus current
 - e. Control bus voltage
 - f. Control bus current
 - g. Temperatures of zone one, zone two, and zone three.

A data point contains all information a. through g. for one day.

The satellite number is inputted during each analysis run. Flight data, extracted from telemetry output printouts, is first punched onto paper tape (providing a hard copy of data) to digitize it and is then read into long-term disc storage files. When a satellite is analyzed, the flight data are called from disc storage and automatically included in the basic analysis program. Updating is accomplished by appending the new data to the old data file.

3. Control elements are inputted during an actual run upon computer request for the needed information. The control elements determine the number of data points analyzed, the type of analysis desired (present options are either total satellite analysis or individual cell analysis) and iteration check criteria in the

computation of degradation factors.

Compute Elements (see 3.5.3 for detailed calculation)

Satellite Analysis

If only satellite analysis is specified, loop (1) will be traversed once for each data point entered. When all N points have been analyzed, the loop is exited and the theoretical power, actual power, the difference between theoretical and actual power, and the number of days from launch is outputted for each data point.

CELL Analysis

If cell analysis has been requested in the input, several data computation loops are traversed for each day analyzed.

On the first pass through the basic compute path, where satellite power is computed from the approximate solar cell equation, degradation factors are set equal to one (1). Testing the difference current and finding the difference does not meet the inputted criteria "B" forces operation through loop (2). Here the degradation factor of I_{SC} (77°F) is updated to a value less than its previous value (see 3.5.3 for details) and the basic compute path is entered again. The degradation factor will be reduced on successive passes around loop (2) until the difference between theoretical and actual current is less than criteria "B". When the difference is in fact less than "B", which is small enough to assure in the iteration scheme acceptable "zero" difference, the present value of the degradation factor is retained. With this degraded I_{SC} (77°F), a similar iteration through loop (3) produces a degraded V_{OC} (77°F). Both degradation factors for I_{SC}

and V_{OC} are outputted and the next data point is analyzed as just described. The program is terminated either by direct command or when all data points have been analyzed.

It should be noted that safeguard alarms are built into each iteration scheme to indicate non-convergence. On no occasion has the alarm been necessary, and differences converge in seven or less iterations.

Output Elements

The analysis program provides two types of output. A tabular list of output data are generated during the run. Also a data file on the magnetic disc is developed simultaneously in a form suitable for input to the plotting routine which is used to generate plots shown in Figures 4-1 through 4-14, and to allow statistical analysis to be implemented on the resulting outputted points at a later date.

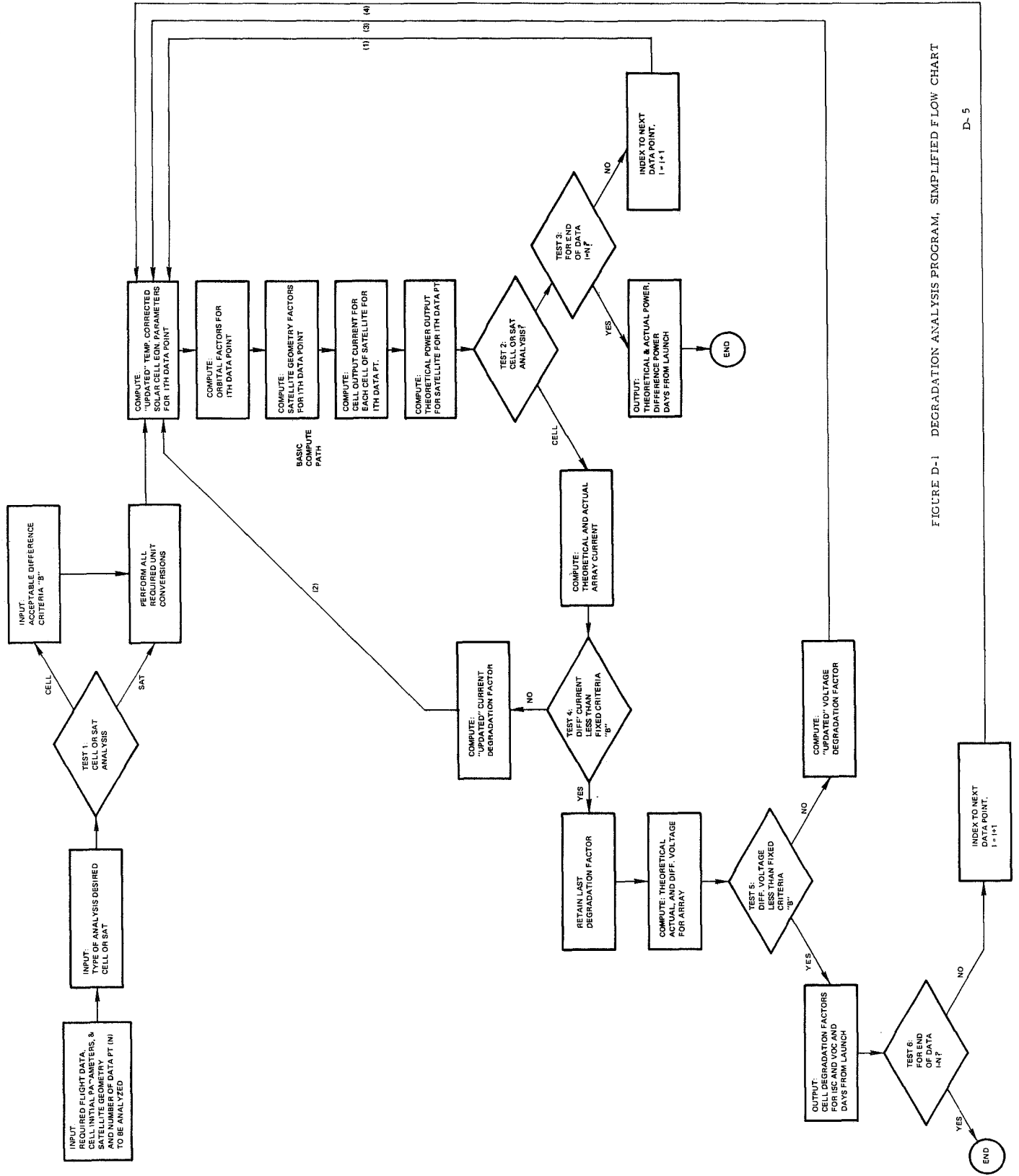


FIGURE D-1 DEGRADATION ANALYSIS PROGRAM, SIMPLIFIED FLOW CHART

PHILCO 

SPACE & RE-ENTRY SYSTEMS DIVISION
Philco-Ford Corporation
Palo Alto, California 94303

